Research Square

Preprints are preliminary reports that have not undergone peer review.
They should not be considered conclusive, used to inform clinical practice,
or referenced by the media as validated information.

Mechanism-Guided Discovery of a Blue-Light Receptor Clade

Andreas Möglich

andreas.moeglich@uni-bayreuth.de

University of Bayreuth https://orcid.org/0000-0002-7382-2772

Lukas Ott

University of Bayreuth

Américo Ranzani

University of Bayreuth

Marius Blackholm

University of Bayreuth

Annabelle Kamitz

University of Bonn

Christian Renzl

Universität Bonn https://orcid.org/0000-0003-2296-1825

Ole Bundgaard

University of Bayreuth

Chongyao Wei

Technical University Dortmund https://orcid.org/0009-0008-6704-8558

Andrés García de Fuentes

University of Bayreuth https://orcid.org/0000-0002-0072-4725

Tom Krebel

University of Bayreuth https://orcid.org/0009-0001-9222-8453

Carlo Unverzagt

University of Bayreuth

Igor Schapiro

Technical University Dortmund https://orcid.org/0000-0001-8536-6869

Günter Mayer

University of Bonn https://orcid.org/0000-0003-3010-4049

Article

Keywords: flavin, light-oxygen-voltage, mechanism, optogenetics, photochemistry, sensory photoreceptor

Posted Date: November 22nd, 2026

DOI: https://doi.org/10.21203/rs.3.rs-11573698/v1

License: This work is licensed under a Creative Commons Attribution 4.0 International License.
Read Full License

Additional Declarations: There is **NO** Competing Interest.

Mechanism-Guided Discovery of a Blue-Light Receptor Clade

Lukas Ott[1], Américo T. Ranzani[1], Marius Blackholm[1], Annabelle Kamitz[2], Christian Renzl[2,3], Ole Bundgaard[4], Chongyao Wei[5], Andrés García de Fuentes[1], Tom Krebel[1], Carlo Unverzagt[4], Igor Schapiro[5], Günter Mayer[2,3], Andreas Möglich[1,6,7,*,‡]

[1] Department of Biochemistry, University of Bayreuth, 95447 Bayreuth, Germany.
[2] Life and Medical Sciences (LIMES), University of Bonn, 53121 Bonn, Germany.
[3] Center of Aptamer Research & Development, University of Bonn, 53121 Bonn, Germany.
[4] Bioorganic Chemistry, Department of Chemistry, University of Bayreuth, 95447 Bayreuth, Germany.
[5] Theoretical Biophysics, University of Dortmund, 44227 Dortmund, Germany.
[6] Bayreuth Center for Biochemistry & Molecular Biology, Universität Bayreuth, 95447 Bayreuth, Germany.
[7] North-Bavarian NMR Center, Universität Bayreuth, 95447 Bayreuth, Germany.

* for correspondence: andreas.moeglich@uni-bayreuth.de
‡ ORCID identifiers: L.O. 0009-0005-9162-0508; A.T.R. 0000-0002-6203-9467; M.B. 0000-0001-8008-1418; A.K. 0009-0005-5901-4890; C.R. 0000-0003-2296-1825; O.B. 0009-0006-1204-3106; C.W. 0009-0008-6704-8558; A.G.F. 0000-0002-0072-4725; T.K. 0009-0001-9222-8453; C.U. 0000-0001-6492-1747; I. S. 0000-0001-8536-6869; G.M. 0000-0003-3010-4049; A.M. 0000-0002-7382-2772

Abstract

Across organisms, sensory photoreceptors decode light stimuli into vital physiological adaptations. Light-oxygen-voltage (LOV) photoreceptors specifically harness a blue-light-induced, reversible carbon-sulfur photoadduct between their flavin chromophore and a conserved cysteine for signal transduction. Here, we identify the LOVme photoreceptor clade that instead implement an irreversible methionyl-flavin carbon-carbon photoadduct as an alternative mechanism. As revealed by structure and function, both photoadduct types converge on the same downstream responses, and hence canonical LOV receptors can be reprogrammed into the LOVme variety. LOVme receptors not only afford sustained light responses, but also, they allow freezing the otherwise transient signaling state of the receptor for in-depth molecular characterization. Though rare, LOVme receptors recur in nature and likely mediate blue-light responses as we exemplify.

Keywords

flavin; light-oxygen-voltage; mechanism; optogenetics; photochemistry; sensory photoreceptor

Introduction

Organisms harness sensory photoreceptor proteins to translate environmental light cues into adaptations of physiology, development, and lifestyle [1,2]. Photoreceptors double as genetically encodable actuators in optogenetics to unlock the acute control by light of cellular state and processes [3,4]. These aspects are borne out by light-oxygen-voltage (LOV) receptors, a flavoprotein family originally identified in plants but also recurring across bacteria and fungi [5–7]. Beyond regulating pivotal biological processes in nature, e.g., plant phototropism and stomatal opening, LOV receptors underpin numerous optogenetic strategies for the precision control of diverse cellular parameters and entities [8]. Absorption of UV-A and blue light by a flavin-nucleotide chromophore in its quinone form drives the reversible LOV photocycle [9,10] (Suppl. Fig. 1a). Upon photoexcitation, the flavin traverses short-lived electronically excited intermediates prior to populating its triplet state, out of which a covalent adduct arises between the flavin C4a atom and the Sγ atom of a conserved cysteine within the LOV receptor. While competing models have been invoked for adduct formation [11–14], the radical-pair mechanism emerges as the most likely [12]. Concomitant with thioadduct formation, the flavin N5 atom protonates and thereby prompts the amide sidechain of a proximal glutamine residue to flip [9,15]. In turn, hydrogen-bonding rearrangements propagate through the LOV receptor to ultimately modulate its biological activity. For the model LOV2 domain from *Avena sativa* phototropin 1 (*As*LOV2) [16] specifically, these reactions culminate in the reversible unfolding of two α helices flanking the LOV core domain (Suppl. Fig. 1b-e). The metastable cysteinyl-flavin Sγ-C4a adduct thermally ruptures in a base-catalyzed reaction, thereby returning the receptor to its original dark-adapted state and completing the reversible photocycle. Irrespective of the prominent roles of the conserved cysteine and glutamine, neither is strictly required for LOV signal transduction [17,18]. Bereft of said cysteine [17], LOV receptors undergo reversible photoreduction to their neutral semiquinone

(NSQ) which is capable of eliciting downstream responses owing to its N5 protonation. Flavin protonation at the N5 position has proven both necessary and sufficient for LOV signal transduction [17,18].

Here, we report a hitherto unknown mode of LOV signal transduction not involving the conserved cysteine but relying on a methionine residue situated close-by the chromophore. Triggered by blue light, an irreversible carbon-carbon adduct manifests between the flavin C4a position and the methionine Cε carbon atom. In contrast to the canonical cysteine, the methionine intriguingly attacks the *re* face of the flavin rather than its *si* face. That notwithstanding, formation of the methionyl-flavin Cε-C4a photoadduct also incurs N5 protonation and thus renders these receptors, dubbed LOVme, signaling-competent. We deliberately install the irreversible LOVme photochemistry into several LOV receptors while maintaining stringent and, in some cases, even improved signaling responses. Though rare, receptors with the LOVme sequence signature occur in nature where they potentially mediate blue-light responses as we ascertain for one specimen. LOVme receptors thus constitute a previously unidentified blue-light receptor clade. Transcending nature, canonical LOV receptors can be converted into irreversible LOVme derivatives at will to unlock persistent cellular responses, e.g., for optogenetics. Moreover, the transient signaling state of LOV receptors that often complicates or altogether eludes molecular characterization can be thereby preserved and unlocked for in-depth investigation.

Results

An Irreversible Photoadduct in Light-Oxygen-Voltage Receptors

To perturb the midpoint potential for the chemical two-electron reduction of the flavin-mononucleotide (FMN) chromophore, we previously placed methionine residues throughout the *As*LOV2 domain [19]. The *As*LOV2 F494M variant with phenylalanine 494 exchanged for methionine (Fig. 1a) retained formation of the canonical cysteinyl-flavin photoadduct, as evidenced by the emergence of a broad absorbance peak around 385 nm under blue light (470 nm). Unlike wild-type

*As*LOV2 (Fig. 1b), this variant, however, unexpectedly failed to fully recover its resting quinone state, even upon prolonged incubation in darkness (Fig. 1c). Rather, iterative illumination-recovery cycles successively depleted the proportion of *As*LOV2 F494M undergoing dark recovery and concomitantly enriched a non-recovering state with an absorbance spectrum similar to that of the conventional cysteinyl-flavin adduct but with 22% reduced oscillator strength and a hypsochromic shift to 376 nm peak absorbance (Suppl. Fig. 2a). Quantitative analysis of these data suggests that during each illumination step, the canonical thioadduct and the non-recovering 376-nm state form in parallel first-order reactions with relative efficiencies of 83% and 17%, respectively (Suppl. Fig. 2b-c).

To determine whether formation of the non-recovering 376-nm state requires the conserved cysteine, we assessed the C450A:F494M variant, denoted as CA:FM in the following, with said cysteine replaced by alanine. Compared to *As*LOV2 wild-type and F494M, the CA:FM variant exhibited an overall similar dark-adapted absorbance spectrum but with less pronounced fine structure for the $S_0 \rightarrow S_2$ transition around 360 nm (Fig. 1d). As for the F494M variant, blue light irreversibly populated the 376-nm state. Notably, a minor population of around 5% underwent a parallel reaction to an intermediate that eventually recovered to the quinone resting state. We tentatively attribute this intermediate to the fully reduced hydroquinone state with diminished absorbance in the visible spectral region [19,20] (Suppl. Fig. 3). Renewed blue-light illumination after recovery irreversibly converted the CA:FM variant to the 376-nm state to essentially full extent.

We next assessed the 376-nm state by chemical denaturation and size-exclusion chromatographic (SEC) analyses. As tracked by absorbance, the protein moiety and the FMN cofactor of *As*LOV2 wild type eluted from the SEC column at around the fifth and tenth volume fractions, respectively, independent of prior exposure to blue light (Fig. 2a). In the case of *As*LOV2 CA:FM, closely similar retention volumes resulted if the sample was kept in darkness prior to denaturation (Fig. 2b). By contrast, when initially exposed to blue light, the FMN cofactor eluted from the SEC column much earlier at around the fifth volume fraction, i.e., alongside the protein component. These

data indicate the formation of a stable photoadduct between FMN and the protein scaffold within *As*LOV2 CA:FM that withstands chemical denaturation. Given that the 376-nm state resembles the conventional cysteinyl-flavin Sγ-C4a thioadduct in its spectral signature (Fig. 1b, d), we suspected that it reflects a photoadduct between the adventitious methionine and the flavin C4a atom. Compared to the cysteinyl-flavin Sγ-C4a thioadduct, a fivefold higher blue-light dose is, however, required for generating the 376-nm photoadduct (Suppl. Fig. 4a-b). With a documented quantum yield of around 40% for conventional thioadduct formation in wild-type *As*LOV2 [21], we estimate the 376-nm photoadduct in the CA:FM variant to arise with around 8% quantum yield.

These findings harken back to earlier studies on the *Chlamydomonas reinhardtii* phototropin LOV1 domain (*Cr*LOV1) [13,22,23]. Replacement of the active-site cysteine by methionine incurred the blue-light-dependent formation of a stable radical state with two broad absorbance maxima between 600 and 700 nm and featuring a photoadduct between the methionine Cε carbon and the flavin N5 atom. Notably, this photoadduct formed in a protracted thermal reaction out of an initial photoproduct maximally absorbing at 415 nm. Regarding their absorbance spectra, neither the photoadduct nor the intermediate hence match the 376-nm photoadduct observed presently for *As*LOV2 CA:FM. To allow more direct comparison, we characterized the corresponding *As*LOV2 CM variant with the active-site cysteine 450 replaced by methionine. Under blue light, *As*LOV2 CM adopted a photoproduct state which, however, differed from that in *As*LOV2 CA:FM by requiring a six-fold higher light dose (Suppl. Fig. 4c) and by maximally absorbing at 346 nm, i.e., spectrally distinct from the 376-nm photoadduct (Suppl. Fig. 5a-b). This 346-nm state converted in a prolonged thermal reaction to a photoproduct state closely resembling the stable radical *Cr*LOV1 Cε-N5 photoadduct in its spectral signature [13,22,23]. Based on this similarity, we assign this photoproduct as the stable Cε-N5 radical photoadduct. As noted before [13,22,23], apart from a bathochromic shift of about 60 nm, the Cε-N5 photoadduct spectrally resembles the NSQ state which reversibly forms in cysteine-deficient LOV modules, e.g., *As*LOV2 C450A (Suppl. Fig. 5c). In marked contrast to the initial 346-nm photoproduct

in *As*LOV2 CM, the 376-nm state of *As*LOV2 CA:FM proved stable over time and did not undergo a comparable spectral evolution.

Piqued by these observations, we probed the effect of UV radiation on the *As*LOV2 CA:FM and CM photoproducts given that the canonical cysteinyl-flavin Sγ-C4a thioadduct photolyzes when exposed to this light quality [24]. Intriguingly, for both the CM and CA:FM variants, the exposure to UV light (390 nm) provoked the formation of the stable Cε-N5 radical state (Suppl. Fig. 6a-b). This state was also populated when the samples experienced blue light before UV exposure (Suppl. Fig. 6c-d). Evidently, *As*LOV2 CA:FM can thus principally assume the Cε-N5 radical photoadduct as well, but under blue light, this reaction is disfavored against the formation of the 376-nm photoadduct.

A Carbon-Carbon Photoadduct Links the Flavin C4a Atom and the Methionine Cε Carbon

Given its differences to the Cε-N5 photoadduct, we characterized the 376-nm photoadduct of *As*LOV2 CA:FM by liquid chromatography coupled to mass spectrometry (Suppl. Fig. 7a-b). The non-illuminated sample eluted as a uniform peak with a discrete mass corresponding to the expected value for the apo-protein (Suppl. Table 1). Following illumination, the elution peak slightly broadened and exhibited an additional species with a mass corresponding to the holo-protein, i.e., *As*LOV2 CA:FM including its FMN cofactor (Suppl. Table 2). Taken together, the data confirm the presence of a stable protein-flavin photoadduct and further suggest that no atom is lost during its formation.

We next crystallized *As*LOV2 CA:FM in its dark-adapted state and determined its three-dimensional structure at 1.09 Å resolution (Suppl. Fig. 8a). Overall, the structure matches that of the wild-type protein [18,25] (Suppl. Fig. 1b) and comprises a five-stranded antiparallel pleated sheet (strands Aβ, Bβ, Gβ, Hβ, and Iβ) surrounded by several α helices (Cα, Dα, Eα, and Fα). Two ancillary helices, centrally engaged in light-dependent signal transduction and denoted A'α and Jα [16], bracket the LOV core fold. Structural differences between *As*LOV2 CA:FM vs. wild type concentrate on the immediate mutation sites. The newly introduced methionine 494 locates to the *re* face of the flavin isoalloxazine instead of the *si* face for the original active-site cysteine in wild-type *As*LOV2 (Fig. 2c-d). Both M494 and the adjacent L496 exhibit multiple conformations, indicative of structural

158 flexibility within this region. The FMN cofactor is coordinated by the same residues as in the wild-
159 type protein, e.g., N482, N492, and Q513, and its location relative to the protein scaffold is
160 unchanged.

161 By irradiating the dark-grown crystals with blue light before cryo-cooling and diffraction
162 measurements, we also elucidated the structure of *As*LOV2 CA:FM in a pseudo-light state at 1.06 Å
163 resolution (Fig. 2e-f, Suppl. Fig. 8b). Intriguingly, the electron density reveals a carbon-carbon
164 photoadduct between the flavin C4a atom and the Cε carbon atom of M494. To accommodate
165 photoadduct formation, the M494 sidechain rearranges as does that of the neighboring L496, with
166 both residues adopting several rotamers. Within the methionyl-flavin Cε-C4a photoadduct, the FMN
167 plane tilts away from M494 by about 4°, which largely recapitulates the motion undergone by this
168 cofactor upon cysteinyl-flavin Sγ-C4a thioadduct formation in wild-type *As*LOV2 (Suppl. Fig. 9a-b).
169 The CA:FM pseudo-light structure immediately rationalizes several of the above observations. First,
170 the CA:FM photoadduct chemically differs from the methionyl-flavin Cε-N5 adduct reported earlier
171 for *Cr*LOV1 [13,22,23] and presently for *As*LOV2 CM which accounts for the divergent absorption
172 spectra above (Fig. 1d, Suppl. Fig. 5). Second, the CA:FM photoadduct rather involves the flavin C4a
173 atom which explains its spectral similarity to the conventional cysteinyl-flavin photoadduct engaging
174 the same carbon atom (Fig. 1b, d). Third, unlike the conventional Sγ-C4a thioadduct, the CA:FM Cε-
175 C4a photoadduct, however, entails carbon-carbon bond formation which accounts for its remarkable
176 stability.

177 The Lewis structure of the methionyl-flavin photoadduct implies flavin N5 atom protonation
178 upon light exposure (Suppl. Fig. 9c). Additional support for this notion derives from the UV-vis
179 spectroscopic experiments and the mass-spectrometric datum that no atom is lost upon photoadduct
180 formation. This matters given the pivotal role of light-induced flavin N5 protonation for LOV
181 downstream signal transduction [17]. In *As*LOV2 specifically, N5 protonation is processed by the
182 conserved Q513 which undergoes a 180° rotation of its amide sidechain and thereby cues subsequent
183 conformational transitions [15,16,18,25]. Most notably, the *As*LOV2 CA:FM light structure exhibits a

prominent sidechain reorientation of residue N414 situated at the A'α:Aβ junction (Fig. 2e-f, Suppl. Fig. 10). Crucially, prior studies on wild-type *As*LOV2 associated this very N414 rearrangement with downstream signal transduction and identified it as a prelude to the unfolding of the A'α and Jα helices [18,25].

The Methionyl-Flavin Cε-C4a Photoadduct Supports Downstream Signal Transduction

To probe whether *As*LOV2 CA:FM maintains downstream conformational transitions that underlie signal transduction, i.e., chiefly A'α and Jα unfolding, we tracked its response to blue light by circular dichroism (CD) spectroscopy. Within its dark-adapted state, the CA:FM variant showed a CD spectrum consistent with its mixed α/β fold, similar to that of the wild-type protein (Fig. 3a), albeit with an about 25% reduced molar ellipticity (Fig. 3b). Light prompted an irreversible 10% loss of the CD signal at 208 nm in *As*LOV2 CA:FM which contrasts with a fully reversible 30% reduction in wild-type *As*LOV2. That notwithstanding, the CD spectra of the light-adapted forms of CA:FM and wild type largely coincide, suggesting similar structures. To better compare the properties of the canonical cysteinyl Sγ-C4a vs. the methionyl Cε-C4a photoadduct, we conducted corresponding analyses on *As*LOV2 F494M which, as demonstrated above, can form either of the two photoadducts (Suppl. Fig. 11a). Whereas the CD spectrum of the dark-adapted protein largely corresponds to that of wild type, the signal change induced by a single exposure to light is less pronounced at only 10% amplitude. Returned to darkness, the CD signal of the F494M variant recovered almost to its initial state. When subjected to repeat recovery-illumination cycles, the amplitude of the light-induced signal change gradually diminished (Suppl. Fig. 11b-c), reflecting the successive accumulation of the irreversible Cε-C4a adduct.

As a whole, the CD data signify that the CA:FM photoadduct prompts partial unfolding of terminal α helices as in the wild-type receptor but at reduced amplitude. This reduction fundamentally owes to an intrinsic loss of α-helical structure in *As*LOV2 CA:FM compared to wild type even within its pristine state prior to any illumination. This loss can be attributed to replacing the active-site cysteine 450 by alanine rather than the F494M substitution, as indicated by the CD spectrum of

*As*LOV2 C450A (Suppl. Fig. 11d). In other words, the CA:FM variant appears principally capable of transducing light signals, yet it is predisposed towards the signaling state. To distinguish receptors employing the methionyl-flavin Cε-C4a photoadduct from wild-type LOV receptors, we designate them LOVme receptors (LOV methionine-empowered) in the following.

Signal Transduction in LOVme Receptors

We next asked if LOVme receptors can be leveraged for regulating the activity of downstream effectors by light. We first investigated this question in a variant of the RNA-guided DNA endonuclease Cas9 rendered blue-light-sensitive via insertion of iLID [26], an *As*LOV2 derivative, into a surface-exposed loop (Fig. 3c). While DNA binding and cleavage are thereby impaired in darkness, blue light relieves the inhibition and restores activity. A cleavage-deficient derivative, termed iLID-dCas9, no longer cuts but merely binds DNA sequence-specifically and can be repurposed as a transcriptional repressor in *E. coli* for so-called CRISPR interference (CRISPRi) [27]. We initially introduced the CA:FM exchanges into the isolated iLID module and ascertained by absorption and CD spectroscopy, respectively, that an irreversible photoadduct forms under blue light and elicits partial α-helical unfolding (Suppl. Fig. 12). Within the CRISPRi context, iLID-dCas9 mediated a (5.5 ± 0.4)-fold repression of a red-fluorescent reporter gene under blue light compared to darkness (Fig. 3d). Introduction of the CA:FM exchanges largely preserved the light response and thus firmly established that LOVme receptors are fundamentally capable of controlling effector output in blue-light-dependent manner. The slightly diminished (4.1 ± 0.4)-fold dynamic range of light regulation is mainly attributable to a partial relief of dCas9 inhibition in darkness (reflected in reduced reporter fluorescence). Consistent with the *As*LOV2 CD analyses above, the CA:FM exchanges apparently tilt the LOVme receptor towards the light-adapted signaling state.

To assess whether LOVme signaling is specific to *As*LOV2 and its iLID derivative or generalizes to other receptors, we next turned to the LOV histidine kinase YF1 that originates from the fusion of the *Bacillus subtilis* YtvA LOV domain to the FixL histidine-kinase effector from *Bradyrhizobium japonicum* [28]. In darkness, YF1 acts as a net kinase on its substrate protein FixJ, but

in the light, it converts to a net phosphatase. Embedded within the pDusk plasmid [29], YF1 mediates the optogenetic downregulation of target-gene expression under blue light (Fig. 3e). Substituting the active-site cysteine 62 by alanine and leucine 106 (corresponding to F494 in *As*LOV2) by methionine greatly degraded the performance of the optogenetic circuit and lowered the dynamic range of light regulation from an original (6.7 ± 0.7)-fold to a mere (1.5 ± 0.2)-fold (Fig. 3f). Akin to iLID-dCas9, this effect again results from a shift of the YF1 receptor towards its signaling state upon implementing the C62A and L106M (CA:LM) exchanges. On its own, the C62A exchange negatively affected regulation but a reduced response remained which can be ascribed to light-induced NSQ formation in the resultant YF1 variant [17]. Likewise, the L106M substitution alone pushed YF1 towards its light-adapted phosphatase state and lowered the attainable dynamic range of regulation. We speculated that the poor performance of the CA:LM variant can be rescued by deliberately introducing additional modifications into YF1 that favor adoption of the dark-adapted kinase state. To this end, random mutagenesis and fluorescence-based screening pinpointed several variants (Suppl. Fig. 13a), among them CA:LM H129Y featuring the replacement of a histidine within the Jα helix by tyrosine. Notably, this helix feeds into the effector module and undergoes light-induced conformational transitions that directly underpin the regulation of histidine-kinase activity [30–32] (Suppl. Fig. 14). Within the pDusk setup, the CA:LM:HY variant counteracted the detrimental effect of the CA:LM exchanges and afforded a (4.5 ± 0.3)-fold decrease of reporter-gene expression under blue light. For additional insight, we expressed, purified, and characterized YF1 and its CA:LM and CA:LM:HY variants. UV-vis absorption spectroscopy indicated that the original YF1 forms the conventional cysteinyl-flavin Sγ-C4a thioadduct as opposed to CA:LM and CA:LM:HY which both assume the irreversible methionyl-flavin Cε-C4a photoadduct (Suppl. Fig. 13b-d). Enzymatic assays revealed that YF1 phosphorylates its FixJ partner in darkness but converts to its phosphatase state under blue light (Suppl. Fig. 13e). By contrast, the CA:LM variant failed to substantially phosphorylate FixJ, irrespective of illumination and consistent with the pDusk reporter-gene experiments. CA:LM:HY

phosphorylated FixJ in darkness and responded to blue light with a reduced kinase activity. Compared to the original YF1, the efficiency of regulation, however, remained impaired.

Given that both iLID-dCas9 and YF1 are engineered LOV receptors, we next investigated whether LOVme signal transduction can also operate in a naturally occurring photoreceptor. To this end, we turned to *Nakamurella multipartita* PAL that sequence-specifically binds a short RNA hairpin, termed aptamer in the following, when activated by blue light [33]. Of advantage, PAL not least underpins the pCrepusculo setup [34] that affords blue-light-dependent regulation of bacterial gene expression and thus provides a readily assayable readout (Fig. 4a). Within this context, wild-type PAL elicited a (9.8 ± 0.4)-fold repression of a red-fluorescent reporter under blue light (Fig. 4b). Reminiscent of YF1 above, the replacement of the active-site cysteine 284 by alanine impaired the PAL light response but did not entirely abrogate it. Introduction of methionine in place of phenylalanine 328 decreased the dynamic range of light regulation to only (3.4 ± 0.4)-fold, caused by predisposing the underlying PAL receptor towards its RNA-binding state already in darkness, again consistent with the YF1 scenario above. This effect is even more manifest upon combining the C284A and F328M substitutions in the CA:FM variant which exhibited overall low reporter fluorescence, indicative of RNA binding, and a much-diminished light response of (2.6 ± 0.2)-fold. As for YF1, we reasoned that additional residue substitutions may counteract the shift towards the RNA-binding state and thereby restore the light response. We identified several PAL variants with restored light responses that bear one or two additional mutations within their LOV modules beyond the CA:FM substitutions (Suppl. Fig. 15). Intriguingly, within pCrepusculo, several of these variants gave rise to strong repression of reporter fluorescence under blue light and outperformed wild-type PAL in its regulatory response. We subsequently focused on a PAL CA:FM variant, termed LOVme-PAL, that harbors a substitution of valine 310 by alanine and displays a (36.2 ± 3.4)-fold regulatory response (Fig. 4b).

Next, we quantified the interaction of LOVme-PAL with its cognate RNA aptamer at the level of the isolated protein [34,35] (Fig. 4c, Suppl. Fig. 16). Analyses by fluorescence anisotropy revealed

that LOVme-PAL binds the aptamer with weak affinity in darkness (K_d = (1.2 ± 0.7) µM) that ramps up by around 80-fold in the photoadduct state (K_d = (16 ± 3) nM) (Fig. 4c). Although somewhat less pronounced than in the wild-type receptor [34,35], LOVme-PAL evidently elicits stringent downstream signaling responses.

Prompted by these findings, we asked whether LOVme-PAL supports optogenetic applications in mammalian cells. Expressed in HeLa cells, both wild-type PAL and LOVme-PAL showed green fluorescence originating from their FMN chromophore (Fig. 4d, Suppl. Fig. 17). Photobleaching with strong blue light diminished the fluorescence owing to photoadduct formation. Upon subsequent incubation in darkness for several minutes, the fluorescence of wild-type PAL recovered to its original levels but that of LOVme-PAL did not, reflecting the irreversible nature of its methionyl-flavin Cε-C4a photoadduct. We next leveraged LOVme-PAL for the optoribogenetic regulation of gene expression by embedding its cognate aptamer within the 5'-untranslated region of an mRNA encoding a luciferase reporter (Suppl. Fig. 17d). For both wild-type PAL and LOVme-PAL, the initial reporter luminescence upon 12 h incubation in darkness dropped by about 13-fold following subsequent 12 h incubation under blue light (Fig. 4e). The ensuing return to darkness for 12 h restored the luminescence signal almost to its initial level for the wild-type receptor. By contrast, cells expressing LOVme-PAL retained severely suppressed luminescence at around 30% of the initial level. We ascribe the partial restoration of the luminescence to cellular turnover and new production of LOVme-PAL rather than actual recovery from the Cε-C4a photoadduct state. Principally, LOVme receptors can hence operate in mammalian cells and evoke long-lasting downstream responses.

Discovery of LOVme Receptors in Nature

Informed by the elucidation of LOVme photochemistry, structure, and signal transduction, we investigated whether such receptors also exist in nature. A sequence search against the non-redundant entries in GenBank for LOV receptors lacking the canonical cysteine (corresponding to *As*LOV2 C450) but possessing a methionine in the position equivalent to *As*LOV2 F494 uncovered around 50 candidate proteins, mostly of prokaryotic provenance (Fig. 5a, Suppl. Fig. 18 and 19a). Multiple

sequence alignments reveal closely similar consensus sequences for the LOVme candidates and regular LOV receptors (Suppl. Fig. 19b), excepting the active-site cysteine and the adventitious methionine.

The mere occurrence of genes in nature with the LOVme hallmarks begs the fundamental question whether at least certain of the encoded receptors can mediate blue-light-dependent signal transduction. We selected for further study a gene from a *Rubrobacteraceae* bacterium that, based on sequence homology, encodes a LOVme-GGDEF-EAL receptor. Notably, GGDEF and EAL are bacterial enzymes responsible for making and breaking, respectively, the widespread second messenger cyclic-di-guanosine monophosphate (c-di-GMP) [36]. Following heterologous expression in *E. coli* and purification, we first analyzed the isolated LOVme module by absorption spectroscopy (Fig. 5b). Exposure to blue light led to the irreversible population of a photoproduct which, based on the spectral similarity to *As*LOV2 CA:FM (Fig. 1d), we assign to a methionyl-flavin Cε-C4a photoadduct. Given that neither the full-length receptor nor a C-terminally truncated LOVme-GGDEF construct could be purified in soluble form, we assessed enzymatic activity and light responses by c-di-GMP-mediated biofilm formation in *E. coli* [37,38]. As many other bacteria, *E. coli* produces biofilms that can be visualized due to their strong binding of certain dyes, e.g., Congo Red (Fig. 5c, Suppl. Fig. 20a-e). Bacteria expressing the full-length LOVme-GGDEF-EAL receptor exhibited more pronounced red coloration, indicative of biofilm formation, following incubation under blue light compared to darkness. Likewise, a receptor variant omitting the C-terminal EAL phosphodiesterase also mediated light-activated biofilm formation, as did a canonical LOV-GGDEF enzyme from a methylotrophic bacterium included as a control [37,38]. By contrast, no red coloration manifested for the isolated LOVme domain.

We also assessed whether the *Rubrobacteraceae* LOVme module can control the output of heterologous effectors and integrated it into the YF1 histidine kinase in lieu of the original, canonical LOV sensor entity. Within the pDusk context, the resultant LOVme-YF1 receptor afforded highly stringent light responses (Fig. 5d). Intriguingly, LOVme-YF1, however, induced reporter expression

by (38.2 ± 2.0)-fold under blue light rather than decreasing it as for the original YF1. Although the molecular origins of the inverted response remain unclear, the LOVme module can evidently interface with heterologous effector modules. Efforts directed at implementing the canonical LOV photochemistry in LOVme-YF1 failed, as installing the active-site cysteine caused gross loss of activity and light responses (Suppl. Fig. 20f). Neither did the additional replacement of the adduct-forming methionine by aliphatic residues restore the response.

Discussion

Photoreception by LOVme Receptors

Our results demonstrate that photoexcitation by UV-A and blue light renders the quinoid flavin chromophore of LOV receptors capable of entering carbon-carbon and carbon-nitrogen photoadducts with close-by methionine residues. As opposed to the metastable cysteinyl-flavin Sγ-C4a bond of canonical LOV receptors, these photoadducts do not recover to the initial quinone state but persist *per se* or irreversibly evolve into other stable states. As shown previously [22,23] and presently for phototropin LOV domains, the exchange of the active-site cysteine for methionine eventually gives rise to a stable flavin radical photoadduct with a covalent Cε-N5 bond to the methionine. By contrast, a methionine abutting the flavin on its opposite *re* side preferentially enters a Cε-C4a photoadduct although it can principally adopt the Cε-N5 radical state, too.

The light-driven formation of the methionyl-flavin Cε-C4a adduct reminds of the photoredox reactions underlying methionine photolabeling, a subject of both experimental and theoretical studies [39,40]. Informed by these findings, we propose a mechanism for LOVme photoadduct formation (Fig. 6a). In its electronic S_0 ground state, the quinoid FMN chromophore is essentially inert towards methionine as it acts at most as a weak oxidant. As a case in point, the midpoint potential for the two-electron reduction to the flavin hydroquinone is around –278 mV (against the normal hydrogen electrode) in *As*LOV2 [19]. Electronic excitation, however, renders the flavin chromophore a potent oxidant with greatly upshifted midpoints, e.g., around +1.4 V to +2.2 V for the one-electron reduction

364 to the semiquinone [41]. Crucially, these values suffice for abstracting an electron from an adjacent
365 methionine sulfur atom, given a reduction midpoint potential for its oxidation to the radical cation of
366 around +1.1 V to +1.9 V, depending upon protein context [42]. Concomitant with methionine oxidation,
367 the flavin reduces to the anionic semiquinone (ASQ) radical state. The initial methionine thiyl radical
368 cation subsequently stabilizes via α deprotonation to form a neutral α-thio radical centered on the Cε
369 atom. Formally, the flavin ASQ could serve as the proton acceptor and thereby convert to the NSQ.
370 Proton transfer may be facilitated by transient water influx as previously inferred [18] and recently
371 documented for *Cr*LOV1 [14]. Lastly, the LOVme thioadduct arises by recombination of the methionyl-
372 flavin radical pair.

373 The mechanistic model begs the question why the LOVme photoadduct preferentially engages
374 the flavin C4a rather than the N5 atom [13]. We propose that the regioselectivity of the radical
375 recombination primarily owes to steric constraints inside the LOV core and specifically the relative
376 distances between the atoms involved: Within dark-adapted *As*LOV2 CA:FM (see Fig. 2c), the flavin
377 C4a and N5 atoms are equidistant from residue 450 (evaluated for the Cα atom), but residue 494 is
378 closer to the C4a atom by 0.3 Å than to N5.

379 We note that the photochemical mechanism presently envisioned aligns with the radical-pair
380 mechanism advanced for formation of the regular cysteinyl-flavin Sγ-C4a photoadduct in
381 conventional LOV receptors [12], which has been recently challenged [14]. Though circumstantial, our
382 investigation now provides strong support for validity of the radical-pair mechanism in the canonical
383 LOV photocycle. Considered together, a unifying reaction model emerges (Suppl. Fig. 21).
384 Photoexcitation empowers the flavin cofactor to oxidize nearby sulfur atoms of adjacent residues, be
385 it cysteine, be it methionine; the resultant sulfur radical cation then stabilizes by deprotonation,
386 followed by recombination with the flavin semiquinone radical to form a covalent adduct.

LOVme Receptors in Nature and the Laboratory

The emergence of a covalent bond to the C4a atom rather than the N5 atom in LOVme receptors has the important consequence of causing flavin protonation at the N5 position which represents a fulcrum in LOV signal transduction [9,15,17,18]. Structural and functional data pinpoint essentially identical downstream responses, irrespective of the pertinent cysteine and methionine residues attacking the flavin isoalloxazine from opposite sides. While the LOVme photochemistry can be thus installed into canonical LOV receptors, we consistently find the efficiency of light-dependent signal transduction to initially drop. Specifically, the removal of the active-site cysteine and, to lesser extent, the methionine introduction predispose the LOV receptor towards its signaling state already in the absence of light. As we showcase, this generally undesirable effect can be counteracted by additional residue replacements that shift the dynamic equilibrium between different receptor states [43,44] back towards the resting conformation.

Though we originally identified LOVme signal transduction in mutant variants of canonical LOV receptors, nature apparently went there first. Comparative sequence analyses of canonical LOV receptors vs. naturally occurring LOVme candidates reveal largely similar consensus sequences barring the positions of the adduct-forming cysteine and methionine residues. As confirmed for the *Rubrobacteraceae* LOVme-GGDEF-EAL receptor, at least certain LOVme candidates are capable of processing blue-light signals into altered biological output, e.g., enzymatic activity. However, it is as-of-yet unresolved whether they genuinely act as blue-light receptors in their native environs in their organisms of origin. That notwithstanding, the question arises which particular organismal requirements might mandate the LOVme mechanism rather than the much more widespread and apparently successful canonical LOV photochemistry. Though entirely hypothetical, one reason could be the irreversible nature of the LOVme methionyl-flavin Cε-C4a photoadduct. By contrast, the canonical LOV photocycle entails a reversal in the dark to the original resting receptor state. Although canonical LOV receptors exhibit a wide spread of timescales for the dark-recovery reaction [45], the exponential time-course of this reaction inevitably means that at least a small receptor proportion

regains its dark-adapted state comparatively swiftly. Against this backdrop, LOVme signaling holds the potential of supporting particularly stringent and persistent responses.

Beyond their roles in nature – largely uncharted as of now –, we identify principal areas that LOVme receptors immediately impact on. As presently exemplified for three disparate systems, originating from plants and bacteria, canonical LOV receptors may be generally amenable to implementation of the irreversible LOVme photochemistry and signal transduction. One scenario where this matters is the application of these receptors as light-gated actuators in optogenetics and biotechnology. Crucially, the irreversible LOVme photochemistry now furnishes sustained, long-lasting cellular responses (see, e.g., Fig. 4e). Not least, LOVme receptors could prove decisive for the optogenetic analyses of developmental processes, e.g., for cell-lineage tracing, conceptually similar to the use of photoactivatable fluorescent proteins in this capacity [46]. While certain other sensory photoreceptor classes also undergo irreversible light responses [47], they are currently limited to specific use cases. By contrast, a specific attraction of the LOVme strategy is that it can be directly installed as an upgrade into numerous, highly versatile LOV receptors already available for the control of manifold cellular processes [8]. Alternatively, light-gated proteins may be constructed from scratch using functional LOVme modules as building blocks (see, e.g., Fig. 5d).

The mechanistic investigation of photoreception and signal transduction is another field standing to benefit from the LOVme arrival. That is because the molecular characterization of the metastable signaling states of sensory photoreceptors is generally complicated by their transient nature. Installing the irreversible LOVme photochemistry now affords a means of preserving and thereby populating the signaling state up to essentially full extent. Not least, this approach particularly applies to the elucidation of photoreceptor structures in their signaling states at atomic resolution.

Implications for Signal Transduction and Beyond

LOVme signaling can be rationalized as a photochemical reaction series culminating in flavin N5 protonation. LOVme receptors thus add to the rich tapestry of molecular strategies by which flavin-binding receptors convert signal input into physiological output, that often hinge on N5 protonation

changes as the common denominator. Changes in oxidation state and protonation are also integral to the multi-facetted roles of isoalloxazine as a redox cofactor in enzyme catalysis. Our findings thus reinforce the notion that flavin-binding photoreceptors, like LOV but also BLUF and cryptochrome receptors, may find their evolutionary origins in metabolic enzymes using flavin-nucleotide cofactors for redox catalysis [17,18]. Arguably, more modes of flavin-centric signal transduction still await discovery in nature or generation by protein engineering. Our work specifically identifies a strategy by which light sensitivity might be conferred onto intrinsically light-insensitive flavin-binding proteins. Judiciously placed methionines stand to enable the formation of methionyl-flavin Cε-C4a, Cε-N5, and potentially other adducts under blue light. Likely, these photoadducts are detrimental to regular function and irreversibly incapacitate the cofactor, thus effectively rendering the flavoprotein in question light-responsive.

Methods

Molecular Biology

*As*LOV2 and iLID variants with residue substitutions were constructed in the background of a pET-19b expression plasmid [19] by PCR amplification and blunt-end ligation. Likewise, the corresponding residues were replaced within the iLID moiety of the chimeric iLID-dCas9 encoded on a pCDF plasmid also bearing tandem gRNAs directed against *Ds*Red (Gelfert *et al.* unpublished).

Again using PCR amplification and blunt-end ligation, PAL variants with residue exchanges were generated within the pCrepusculo-*Ds*Red reporter context [34]. An expression construct for PAL C205A:C284A:V310A:F328M was created by Gibson assembly [48] using the earlier pET-19b-SUMO-PAL expression plasmid [34] and the pertinent pCrepusculo-*Ds*Red plasmid as templates.

Residue replacements within YF1 were prepared within the pDusk-*Ds*Red reporter [29] and the pET-41a expression [30] vectors via PCR amplification with mismatch primers followed by *Dpn*I digest.

Synthetic genes encoding residues residues 1-582 of the *Rubrobacteraceae* LOVme-GGDEF-EAL receptor (Genbank identifier CAA9447600.1) and residues 1-314 of *Ms*LadC from

464 *Methylotenera* sp. [38], respectively, were procured from GeneArt (Regensburg) with codon usage
465 adapted to *Escherichia coli*. Both genes were subcloned into pET-19b plasmids by Gibson assembly
466 and thereby equipped with an N-terminal His_6-SUMO tag and placed under the control of a T7-*lacO*
467 promoter. Truncations of the LOVme receptor comprising residues 1-138 and 1-314, respectively,
468 were obtained by PCR amplification and blunt-end ligation. The LOVme module (residues 1-138)
469 was introduced into pDusk-*Ds*Red by Gibson assembly to replace the original LOV domain from
470 *Bacillus subtilis* YtvA [29].

471 Oligonucleotide primers were purchased from Integrated DNA Technologies (Leuven,
472 Belgium). All constructs were verified by Sanger sequencing (Microsynth AG, Göttingen)

473 **Gene Expression and Protein Purification**

474 Gene expression was generally conducted in *E. coli* CmpX13 [49] or LOBSTR bacteria [50] harboring the
475 requisite expression plasmid. Cells were grown at 37°C and 225 rpm agitation in lysogeny broth (LB)
476 medium supplemented with kanamycin (50 µg mL^{-1}) and, in the case of the CmpX13 strain,
477 additionally 50 µM riboflavin. Gene expression was induced by adding 0.5 to 1 mM isopropyl-β-
478 thiogalactopyranoside (IPTG) once the bacterial culture reached an optical density at 600 nm (OD_{600})
479 of around 0.6-0.8. Incubation continued at 16-18°C for at least 16 hours before cell harvest by
480 centrifugation.

481 The purification of *As*LOV2 variants followed a previous protocol [19]. Briefly, after cell lysis
482 by sonication, the supernatant was cleared by centrifugation and applied to a Co^{2+} immobilized metal
483 ion affinity chromatography (IMAC) column. Bound protein was eluted with imidazole in fractions
484 that were pooled based on protein content and purity as gauged by denaturing polyacrylamide gel
485 electrophoresis (PAGE). Next, the His_6-SUMO tag was cleaved off by overnight incubation at 4°C
486 with SenP2 protease, followed by a second IMAC purification step. Purified *As*LOV2 variants were
487 dialyzed into storage buffer (20 mM tris-(hydroxymethyl)-aminomethane [Tris]/HCl pH 8.0, 20 mM
488 NaCl, 10% [v/v] glycerol), concentrated by spin filtration, rapidly frozen in liquid nitrogen, and stored
489 at –80°C until use. The *As*LOV2 CA:FM protein destined for crystallization was additionally purified

via anion-exchange chromatography. To this end, the sample was eluted from a 1-mL HiTrap Q HP anion exchange column (Cytiva, Freiburg) with a linear NaCl concentration gradient between 50 and 500 mM using an Äkta prime plus system (Cytiva). The isolated LOVme domain was purified likewise but with buffers containing 5 mM $MgCl_2$ and 500 mM NaCl instead of 150 mM. Following the two IMAC steps, the sample was reconstituted with a 20-fold molar excess of FMN (Cayman Chemicals) for 4 h at 4°C. Surplus FMN was removed by passing the sample over a PD10 desalting column (GE Healthcare) and subsequent dialysis against storage buffer.

The YF1 purification employed a previous protocol [30]. After lysis, the supernatant was passed over a Co^{2+}-IMAC column, and bound protein was eluted with 200 mM imidazole. Fractions were pooled based on PAGE analysis, dialyzed into storage buffer (20 mM Tris/HCl pH 8.0, 20 mM NaCl, 10% [v/v] glycerol), concentrated by spin filtration, and stored at –80°C. The FixJ protein was purified as described in [18], similar to the above protocol used for the *As*LOV2 variants. After a first Co^{2+}-IMAC stage, an N-terminal His_6-SUMO was removed by SenP2 digest, followed by a second IMAC step. To aid FixJ solubility, 1 M NaCl was added to all buffers. After PAGE analysis, the protein samples were dialyzed into storage buffer (20 mM Tris/HCl pH 8.0, 250 mM NaCl, 10% [v/v] glycerol), concentrated, and kept at –80°C.

To reduce aggregation caused by disulfide formation, cysteine 205 within the ANTAR domain of PAL was replaced by alanine. The resulting PAL receptor variant with the C205A:C284A:F328M:V310A mutations was then produced similarly to the *As*LOV2 variants. After cell harvest, the cell lysate was purified by two IMAC steps and SenP2 digest as above. Further purification was carried out through anion-exchange chromatography (HiTrap Q HP column) and size-exclusion chromatography (Sephacryl S-200). Based on PAGE analysis, chromatography fractions were pooled, dialyzed into storage buffer (20 mM Tris/HCl pH 8.0, 150 mM NaCl, 10% [v/v] glycerol), concentrated by spin filtration, and stored at –80°C.

Concentrations of the respective LOV receptors were determined by UV-vis spectroscopy based on the FMN cofactor absorbance using a molar extinction coefficient of 12,500 M^{-1} cm^{-1} at the

maximum near 450 nm. For FixJ, an extinction coefficient at 280 nm of 4,860 M^{-1} cm^{-1} was employed [28].

Chromatographic and Mass-Spectrometric Analyses of the Methionine Photoadduct

Protein samples were diluted into 20 mM potassium phosphate pH 8.0, 20 mM NaCl to a concentration of around 100 µM and incubated at 22°C for 20 min in darkness or under 450-nm light at an intensity of 2 mW cm^{-2}. Throughout the work, all light intensities were determined with a model 842-PE power meter and a 918D-UV-OD3 silicon photodiode (both from Newport, Darmstadt). Following 6-fold dilution into 6 M guanidinium chloride, samples were applied to a PD10 column equilibrated with 6 M guanidinium chloride before elution with the same buffer in 600-µL fractions. UV-vis absorbance spectra of the elution fractions were recorded on an Agilent Cary 3500 spectrophotometer.

The *As*LOV2 CA:FM photoadduct was also analyzed by mass spectrometry. To this end, 15 µM protein were incubated at 22°C for 10 min in darkness or under 450-nm light (2 mW cm^{-2}). Samples were then diluted into 0.1% formic acid and analyzed on a Waters ACQUITY H-Class Ultimate 3000 UHPLC with a diode-array detector coupled to a micro-mass LCT ESI-TOF-mass spectrometer (Thermo Fisher Scientific, Dreieich). The chromatographic separation was performed on a SupelcoDiscovery BIO Wide Pore C5 column (50 × 2.1 mm, 3 µm, 300 Å) at 40°C and a flow rate of 0.5 mL min^{-1} using the mobile phase A (0.1% formic acid) and B (acetonitrile/0.1% formic acid). After isocratic elution for 1.25 min at an A:B ratio of 95:5, the concentration of B was linearly increased to 95% over 9 min, followed by isocratic elution at this solvent ratio for 2.25 min. The expected molecular weights (*M*) of *As*LOV2 C450A:F494M with and without its FMN cofactor were calculated based on the respective sum formulae $C_{758}H_{1205}N_{212}O_{239}PS_3$ (*M* = 17,239.38 Da) and $C_{741}H_{1184}N_{208}O_{230}S_3$ (*M* = 16,783.03 Da) (Suppl. Tables 1 and 2). The mass peaks observed for the non-irradiated and blue-light-exposed samples are given in Suppl. Tables 1 and 2. Note that for the latter condition, two series of mass peaks resulted, corresponding to the unmodified sample and the photoadduct.

UV-vis Absorption Spectroscopy

Measurements were conducted on Agilent Cary60 and Cary3500 instruments at 22°C as controlled by Peltier thermostats. Spectroscopic analyses were carried out in 20 mM potassium phosphate pH 8.0, 20 mM NaCl for the *As*LOV2 and iLID variants; in 50 mM Tris/HCl pH 8.0, 500 mM NaCl, 5 mM $MgCl_2$ for the *Rubrobacteraceae* LOVme domain; in 20 mM Tris/HCl pH 8.0, 150 mM NaCl, 10% (v/v) glycerol for the PAL variants; and in 20 mM Tris/HCl pH 8.0, 20 mM NaCl, 10% (v/v) glycerol for the YF1 variants. Absorbance spectra were recorded for the dark-adapted samples and after saturating exposure to 450-nm or 470-nm light. To monitor the dark-recovery reaction, samples were returned to darkness immediately after illumination ceased, and the absorbance was continuously tracked over time.

For *As*LOV2 CM and CA:FM, the recovery reaction was additionally observed over extended periods of time. After blue-light exposure (470 nm, 2 mW cm^{-2}, 10 min), the samples were returned to darkness and incubated at 22°C for 168 h. To remove protein aggregates forming over time, the samples were centrifuged for 9 min at 16,000 × *g* before periodically acquiring absorbance spectra.

Relative quantum efficiencies for photoadduct formation in *As*LOV2 wild type vs. CA:FM were determined as described previously [51]. Briefly, 10 µM of either protein were exposed to blue light (470 nm, 2 mW cm^{-2}), and the photoadduct accumulation over time was tracked by absorbance at 450 nm and 470 nm. The resultant absorbance kinetics were evaluated with Fit-o-mat [52] according to single-exponential functions.

16 µM *As*LOV2 F494M were subjected to iterative cycles of blue-light pulses (15 s, 470 nm, 20 mW cm^{-2}) followed by dark recovery for 30 min at 22°C. The reaction progress was monitored by absorbance at 450 nm. As illustrated in Suppl. Fig. 2b, in each illumination cycle, the protein can either form the canonical Sγ-C4a cysteinyl-flavin or the 376-nm photoadducts with unimolecular rate constants of k_P and k_{376}, respectively. As the 376-nm state forms irreversibly, the fraction of molecules returning to the original dark-adapted state D drops with cycle number x by a constant factor according to

$$D(x) = D_0 \cdot \left(1/\left(k_{376}/k_p + 1\right)\right)^x$$

The absorbance decay with increasing cycle number was evaluated according to this model with Fit-o-mat.

To probe the response of *As*LOV2 CM and CA:FM to UV light, around 20 µM of the respective variant in its dark-adapted state were exposed to 390-nm light at 10 mW cm^{-2} intensity, and absorbance spectra were recorded over time. To additionally assess the stability of the blue-light-induced photoadduct, the samples were first illuminated with saturating blue light (470 nm, 2 mW cm^{-2},30 min) before UV-light treatment.

To determine the extent of chromophore incorporation in the *As*LOV2 CA:FM sample subjected to mass-spectrometric analysis, see above, 20 µM of the protein were diluted into 5 M guanidine hydrochloride. UV-vis absorbance spectra were recorded and compared to those of wild-type *As*LOV2 and free FMN in the same solvents. Using molar extinction coefficients under denaturing conditions of 12,500 M^{-1} cm^{-1} at 450 nm for FMN and 9,970 M^{-1} cm^{-1} at 280 nm for the *As*LOV2 apoprotein, the chromophore incorporation was then calculated.

The *As*LOV2 C450A variant was spectroscopically analyzed in the presence of 10 mM Tris(2-carboxyethyl)phosphine (TCEP). UV-vis absorbance spectra were acquired for the dark-adapted form and after illumination with 470-nm light at 20 mW cm^{-2} for 30 minutes. Free flavin mononucleotide was assessed in buffer containing 20 mM of the sacrificial electron donor ethylenediaminetetraacetic acid (EDTA). Following acquisition of a UV-vis absorbance spectrum for the dark-adapted state, the sample was exposed to 470-nm light (20 mW cm^{-2}) for 3 minutes, and another spectrum was recorded. A final spectrum was acquired after subsequent recovery in darkness for 60 minutes.

Circular-Dichroism Spectroscopy

Far-UV circular-dichroism (CD) spectra of the *As*LOV2 and iLID variants were recorded on a JASCO-710 spectrophotometer with Peltier temperature control (JASCO PTC-348WI). All measurements were performed at 22°C in 20 mM potassium phosphate pH 8.0, 20 mM NaCl in quartz cuvettes with 1 mm path length. CD spectra were recorded between 190 and 250 nm for the dark-

adapted samples and after exposure to strong blue light (470 nm, 40 mW cm^{-2}, 5 s). Control UV-vis absorbance measurements confirmed that this light dose suffices for complete population of the light-adapted state. Upon withdrawal of blue light, the variants were incubated in darkness for 10 min before acquisition of another CD spectrum.

For the *As*LOV2 F494M variant, samples were subjected to iterative cycles of blue light (450 nm, 1 W cm^{-2}, 1 s) and 30 min dark recovery at 22°C. After each blue-light or recovery step, far-UV CD spectra were recorded as above.

Structural Biology

*As*LOV2 CA:FM single crystals were produced by sitting-drop vapor diffusion in darkness at 19°C within CombiClover500 plates (Rigaku Reagents). To this end, between 7.5 to 10 mg mL^{-1} protein within 20 mM Tris/HCl pH 8.0, 20 mM NaCl, 10% (v/v) glycerol were mixed at a 1:1 volume ratio with mother liquor. Based on previous reports [18,25], the crystallization buffer contained 0.1 M sodium acetate buffered at pH values between 4.5 and 5.0; 6 to 8% (v/v) polyethylene glycol (average molar weight 4,000 Da); and 30% (v/v) glycerol. Orthorhombic crystals appeared within 1 day. For the determination of the dark-adapted structure, these crystals were mounted in nylon loops (Hampton) under red safe light and rapidly cryo-cooled by immersion in liquid nitrogen. For the light-adapted structure, crystals were illuminated for 2 min with blue light (470 nm, 40 mW cm^{-2}) immediately prior to cryo-cooling. Diffraction data were collected at beamline 14.1 of the BESSY synchrotron. Data collection, processing, and refinement statistics are provided in Supplementary Table 3.

Diffraction data were indexed, integrated, and scaled through the XDSapp interface [53,54]. Structures were solved by molecular replacement with PHASER [55] using the structure of *As*LOV2 as the search model (PDB entry 2v0u [25]). Model building and restraint refinement were done with Coot [56] and Refmac5 [57], respectively. Structural models were validated with MolProbity [58]. Atomic coordinates and structure-factor amplitudes were deposited in the Protein Data Bank under accession codes pdb_000033sp and pdb_000033sq for dark-adapted and light-adapted *As*LOV2 CA:FM,

619 respectively. Structural models were analyzed and molecular graphics were rendered with PyMOL
620 (version 3.1.0a0 Schrödinger, LLC).

621 **Experiments on iLID-dCas9 Variants**

622 All measurements were carried out in *E. coli* CmpX13 cells carrying a pET-28c plasmid that harbors
623 the red-fluorescent *Ds*Red reporter under the control of a T7-*lacO* promoter [29]. Into these cells, pCDF
624 plasmids were transformed that encode two constitutively expressed single-guide RNAs directed
625 against *Ds*Red and an arabinose-inducible expression cassette for a given iLID-dCas9 variant.
626 Triplicate starter cultures were grown overnight in darkness at 30°C in 5 mL LB supplemented with
627 50 µg mL^{-1} kanamycin and 100 µg mL^{-1} streptomycin (LB Kan/Strep). Next, 1 µL of each culture
628 was spotted onto LB Kan/Strep plates containing 200 µM IPTG, followed by incubation in darkness
629 or blue light (450 nm, 70 µW cm^{-2}) for 18 h at 30°C. Upon resuspension in water, the OD_{600} of the
630 cells was measured, followed by determination of the *Ds*Red fluorescence at excitation and emission
631 wavelengths of (554 ± 9) nm and (591 ± 20) nm, respectively. All measurements were performed on
632 a Tecan Infinite M200pro multimode microplate reader (Tecan Group Ltd, Männedorf, Switzerland).
633 Fluorescence readings were divided by OD_{600}, followed by normalization to the signal obtained for
634 the original iLID-dCas9 in darkness. Reported values represent mean ± s.d. of three or more biological
635 replicates.

636 **Experiments on YF1 Variants**

637 YF1 variants were initially generated and tested within the framework of the pDusk-*Ds*Red reporter
638 setup. As previously detailed [29], the light response of a given YF1 variant was assessed by
639 transforming the respective pDusk-*Ds*Red plasmid variant into *E. coli* CmpX13. For each variant,
640 starter cultures were inoculated in 200 µL LB/Kan within individual wells of clear 96-well microtiter
641 plates (MTP). The plates were sealed with gas-permeable film (BF-410400-S, Corning) and incubated
642 in darkness for 18 h at 37°C and 225 rpm agitation. Next, 2 µL of each culture were diluted 100-fold
643 into 198 µL fresh LB/Kan medium within individual wells of two separate MTPs. After sealing, the

MTPs were incubated for 18 h at 37°C and 225 rpm agitation, with one plate being kept in darkness and the other being exposed to 470-nm light (cycles of 10 s light followed by 10 s darkness, resulting in a time-averaged light intensity of 90 µW cm^{-2}) [59]. The optical density at 600 nm (OD_{600}) and the *Ds*Red fluorescence of the cultures were measured and processed as described above. All fluorescence values are divided by OD_{600} and normalized to the value recorded for the original pDusk-*Ds*Red in darkness; they represent mean ± s.d. of four biological replicates.

To enhance the dynamic range of light regulation in the YF1 CA:LM variant, the underlying pDusk-*Ds*Red plasmid was subjected to random mutagenesis. To this end, the gene fragment encoding the *B. subtilis* LOV module (residues 1-147) was amplified by error-prone PCR using Taq polymerase. The error rate was increased by adding 1 mM dCTP, 1 mM dTTP, 5 mM $MgCl_2$, and 50 µM $MnCl_2$ to the standard reaction mix. The resultant DNA fragment was ligated into the pDusk-*Ds*Red backbone by Gibson assembly. Upon transformation into *E. coli* XL1-Blue, bacteria were plated on LB/Kan agar and incubated overnight at 37°C in darkness. Bacterial colonies exhibiting elevated fluorescence relative to the parental YF1 CA:LM variant were isolated and re-streaked onto two fresh LB/Kan plates that were then incubated overnight at 37°C in darkness and under 40 µW cm^{-2} 470-nm light, respectively. Visual inspection identified clones displaying higher *Ds*Red expression under dark than under light conditions. Pertinent clones were analyzed by plasmid isolation and Sanger DNA sequencing. The plasmids were then transformed into *E. coli* CmpX13 followed by analysis of the blue-light response as described above.

The kinase activity of the YF1 variants was further assessed in a coupled fluorescence-anisotropy experiment [18]. A double-stranded DNA substrate comprising the FixK2 operator sequence to which phosphorylated FixJ binds with high affinity was prepared by annealing oligonucleotide primers with the forward primer carrying a (5-and-6)-carboxytetramethylrhodamine (TAMRA) label at its 5' end. The sequence of the DNA was 5'-GAG CGA TAT CTT AAG GGG GGT GCC TTA CGT AGA ACC C-3' where the underlined portion designates the FixK2 operator. Enzymatic assays were performed at 25°C within black MTPs in buffer containing 10 mM 4-(2-hydroxyethyl)-1-

piperazineethanesulfonic acid (HEPES)/KOH pH 7.6, 80 mM KCl, 2.5 mM $MgCl_2$, 0.1 mM EDTA, 10% (v/v) glycerol, 4% (v/v) ethylene glycol, 10 mM TCEP. 2.5 µM of a given YF1 variant were mixed with 25 µM of the response regulator FixJ, 1.25 µM TAMRA-labelled DNA substrate, and 100 µg mL^{-1} bovine serum albumin (BSA). After equilibration at 25°C, the reaction was initiated by addition of 1 mM ATP, and the TAMRA fluorescence anisotropy was tracked over time with a CLARIOSTAR multi-mode MTP reader (BMG Labtech) at emission and excitation wavelengths of (540 ± 10) nm and (590 ± 10) nm, respectively. After around 20 minutes, the measurement was paused to illuminate the samples with 470-nm light for 30 s (30 mW cm^{-2}) before continuing recording data.

Experiments on PAL Variants

Variants of the *N. multipartita* PAL receptor were first created and tested within the pCrepusculo-*Ds*Red plasmid that affords a ready readout on light-dependent RNA binding [33,34]. *E. coli* CmpX13 cells carrying pCrepusculo-*Ds*Red plasmids encoding a given PAL variant were used to inoculate 500 µL LB supplemented with 100 µg mL^{-1} streptomycin (LB/Strep) within individual wells of a 96-deep-well microtiter plate. After sealing with gas-permeable film, the MTP was incubated for 16-18 h at 37°C and 800 rpm agitation. The bacterial cultures were then diluted 100-fold into individual wells of two separate transparent MTPs each containing 200 µL LB/Strep. The sealed plates were then incubated for 24 h at 37°C and 800 rpm agitation in either darkness or under constant blue light (470 nm, 60 µW cm^{-2}). The OD_{600} and the *Ds*Red fluorescence of the cultures were measured and evaluated as described above. Data were divided by OD_{600} and normalized to the readings acquired in darkness for the original pCrepusculo-*Ds*Red system and reflect mean ± s.d. of three biological replicates.

A library of PAL CA:FM variants was generated within the pCrepusculo-*Ds*Red background by random mutagenesis to restore light responsiveness. The region encoding the LOV domain (residues 212–365) was amplified by error-prone PCR using the conditions described above for YF1 and subsequently placed into the pCrepusculo backbone by Gibson assembly. The resulting plasmid library was directly transformed into *E. coli* CmpX13, and transformed cells were plated on LB/Strep agar and incubated overnight at 37°C in darkness. Bacterial colonies displaying higher fluorescence

relative to the parental PAL CA:FM variant were isolated and re-streaked onto two fresh LB/Strep plates, which were incubated overnight at 37°C in darkness and under 40 µW cm^{-2} 470-nm light, respectively. Clones with enhanced light-dependent fluorescence differences were visually identified, isolated, and subsequently analyzed using Sanger DNA sequencing. For eventual measurements, the plasmids were freshly transformed into CmpX13 cells.

To probe the interaction of PAL variants with their RNA substrate, an RNA molecule comprising the so-called motif-3 aptamer [34,35] and 5'-labeled with TAMRA was synthesized (5'-ACC UUC GGU UCA GCA GCG AGC CG-3', Integrated DNA Technologies). All experiments were carried out within black 384-well MTPs in buffer containing 12 mM HEPES/KOH pH 7.7, 135 mM KCl, 10 mM NaCl, 1 mM $MgCl_2$, 10% (v/v) glycerol, 100 µg mL^{-1} BSA, and 0.3 U $µL^{-1}$ RiboLock RNAse inhibitor (ThermoFisher Scientific). A constant 4 nM of the TAMRA-labelled RNA substrate were incubated at 25°C with increasing amounts of dark-adapted PAL, and the TAMRA fluorescence anisotropy was measured as described above. Then, the samples were exposed to saturating blue light (470 nm, 7 mW cm^{-2}) for 5 min, and the fluorescence anisotropy was recorded again. The fluorescence anisotropy data were evaluated as a function of the PAL concentration according to [34]:

$$r = r_0 + r_1/2 \cdot \left(1 + [\mathrm{PAL}]/c_{\mathrm{tot}} + K_{\mathrm{D}}/c_{\mathrm{tot}} - \sqrt{(1 + [\mathrm{PAL}]/c_{\mathrm{tot}} + K_{\mathrm{D}}/c_{\mathrm{tot}})^2 - 4 \cdot [\mathrm{PAL}]/c_{\mathrm{tot}}}\right)$$

where r, [PAL], K_D, and c_{tot} refer to the fluorescence anisotropy; the PAL concentration; the dissociation constant; and the overall amount of labeled RNA in the assay, respectively. Nonlinear least-squares fitting was done with Fit-o-mat.

Experiments to assess the light response of LOVme-PAL in a mammalian context were conducted in HeLa cells (CLS Cell Lines Service) cultured in DMEM medium (high glucose, GlutaMAXTM, Thermo Fisher Scientific) supplemented with 10% (v/v) fetal calf serum and 1% (v/v) antibiotics solution (100 U mL^{-1} penicillin, 100 µg mL^{-1} streptomycin). Cells were cultivated at 37°C and 5% (v/v) CO_2 and were passaged every 2–3 days. To ascertain photoswitching in the mammalian host, 2×10^4 cells were seeded into black 24-well plates with clear glass bottom (µ-plate, ibidi). After 24 h incubation, the cells were transfected with 600 ng pmCherry-PAL or pmCherry-LOVme-PAL

using FuGENE HD (Promega) according to the manufacturer's instructions. After 48 h, cells were analyzed by confocal laser scanning microscopy (LSM 710, Zeiss) to monitor the mCherry (excitation [ex]/emission [em] 543/596–696 nm) and PAL (ex/em 405/488–529 nm) fluorescence, respectively. Similar to before [33], fluorescence was monitored by confocal laser scanning microscopy (LSM 710, Zeiss) in two channels (mCherry ex/em 543/596–696 nm; PAL ex/em 405/488–529 nm) as a time series of 6 frames at 60-s intervals. The photochemistry of PAL was assessed by irradiating the samples through the bleaching tool of the microscope (458-nm argon laser with 100% transmission, 10 iterations with ~ 111 s exposure total). Afterwards, the cells were left to recover in darkness for 10 min before fluorescence was recorded again.

To demonstrate optoribogenetic control of translation, 5×10^4 HeLa cells were seeded into two separate 24-well plates and incubated in darkness at 37°C. After 24 h, the cells were washed, and fresh, pre-warmed medium was added. The cells were then co-transfected with 450 ng pmCherry-PAL or pmCherry-LOVme-PAL and 50 ng pMetLuc reporter with 1.5 µL FuGENE HD (Promega) according to the manufacturer's instructions. Transfected cells were incubated for 36 h at 37°C in darkness with a medium exchange after 24 h. For the luminescence assay, luciferase substrate was dissolved tenfold in buffer according to the manufacturer's instructions (Ready-To-Glow Secreted Luciferase, Takara Clontech), and 5 µL were dispensed into wells of a white 96-well plate (lumitrac200, Greiner). Then, 50 µL cell-culture supernatant were added, and the reaction mixture was incubated for 25 min before measuring the luminescence signal on an Enspire plate reader (PerkinElmer) with an integration time of 1 s. The media was then refreshed to remove secreted luciferase, and the cells were incubated under blue light (465 nm, 106 µW cm^{-2}, cycles of 30 s light, followed by 30 s darkness). Luminescence was measured again as described above, and the media was exchanged once more before incubation of the cells in darkness for 12 h. A final luminescence measurement was performed as described above.

Database Analyses of LOVme Receptors

A BLAST search against the non-redundant entries in GenBank with the *As*LOV2 sequence (Uniprot O49003, residues 404-519) as the template and an expectation value of 10 as the cutoff yielded around 190,000 hits. These hits were filtered for sequences containing at least 9 out of 10 residues highly conserved across the LOV receptor family [60]. In one-letter code, within *As*LOV2 these residues are G447, N449, C450, R451, F452, L453, Q454, N482, N492, and Q513 (see grey highlight in Fig. 5a and Suppl. Fig. 19a). The subsequent filtering for sequences lacking the active-site cysteine but bearing a methionine residue at the position corresponding to F494 in *As*LOV2 identified 53 candidate LOVme receptors (see Suppl. Fig. 19a for identifiers of these receptors). The pertinent sequences were annotated with HMMER [61] using the Pfam [62] domain profiles. Multiple sequence alignments were generated using ClustalX [63] and MUSCLE [64], followed by evaluation with WebLogo [65].

Characterization of a Naturally Occurring LOVme-GGDEF-EAL Receptor

To assess the light response of the *Rubrobacteraceae* LOVme-GGDEF-EAL receptor, we adapted an earlier approach [37]. *E. coli* CmpX13 cells harboring pET-19b expression plasmids encoding either the isolated LOVme domain, the full-length LOVme-GGDEF-EAL receptor, a truncated LOVme-GGDEF construct, or the canonical LOV-GGDEF receptor from *Methylotenera* sp. were grown in darkness at 37°C in 5-mL liquid LB/Kan cultures. Gene expression was induced by addition of 0.1 mM IPTG when the cultures reached an OD_{600} of 0.5. After continuing the incubation for 2 h at 16°C, cells were harvested by centrifugation and resuspended in H_2O to an OD_{600} of 10. 2 µL of each culture suspension were spotted onto two separate LB/Kan plates supplemented with 0.1 µg mL^{-1} Congo Red and 0.1 µg mL^{-1} Coomassie Brilliant Blue G250. Incubation continued for 17 h at 20°C in either darkness or under constant blue-light illumination (470 nm, 20 µW cm^{-2}). Then, the temperature was lowered to 6°C, and the incubation in darkness or under blue light, respectively, resumed for 3 days before photographs of the plates were taken. To quantify the Congo Red staining within the bacterial

colonies, absorbance spectra were recorded in reflectance mode using a SEC 2020 diode-array spectrophotometer (ALS, Tokyo).

Statistical Analyses

Confidence intervals of parameters determined by nonlinear least-squares regression analysis represent the fitted parameter value ± its asymptotic standard error. For reporter-gene assays, multiple biologically independent replicates were analyzed as stated in the figure legends. Dark vs. light differences were evaluated by Welch's two-sided *t* tests with unequal variances as implemented in Microsoft Excel. For multiple pairwise comparisons (Fig. 4e), the *p* values were adjusted using the Bonferroni correction.

Data Availability

Data underlying the main and supplemental figures of the work are available at Zenodo (https://doi.org/10.5281/zenodo.23282460). The LOVme-Dusk plasmid will be available from Addgene under accession number 263226. Atomic coordinates and structure-factor amplitudes for the dark-adapted and the pseudo-light-adapted structures of *As*LOV2 C450A:F494M have been deposited in the Protein Data Bank under accession codes pdb_000033sp and pdb_000033sq. Additional materials are available from the corresponding author upon reasonable request.

References

1. Hegemann, P. Algal sensory photoreceptors. *Annu. Rev. Plant Biol.* **59**, 167–189 (2008).
2. Möglich, A., Yang, X., Ayers, R. A. & Moffat, K. Structure and function of plant photoreceptors. *Annu. Rev. Plant Biol.* **61**, 21–47 (2010).
3. Deisseroth, K. Optogenetics. *Nat Methods* **8**, 26–29 (2011).
4. Nagel, G. *et al.* Channelrhodopsin-1: a light-gated proton channel in green algae. *Science* **296**, 2395–2398 (2002).

5. Huala, E. *et al.* Arabidopsis NPH1: a protein kinase with a putative redox-sensing domain. *Science* **278**, 2120–2123 (1997).
6. Christie, J. M. *et al.* Arabidopsis NPH1: a flavoprotein with the properties of a photoreceptor for phototropism. *Science* **282**, 1698–1701 (1998).
7. Conrad, K. S., Manahan, C. C. & Crane, B. R. Photochemistry of flavoprotein light sensors. *Nat. Chem. Biol.* **10**, 801–809 (2014).
8. Losi, A., Gardner, K. H. & Möglich, A. Blue-Light Receptors for Optogenetics. *Chem. Rev.* **118**, 10659–10709 (2018).
9. Salomon, M. *et al.* An optomechanical transducer in the blue light receptor phototropin from Avena sativa. *Proc. Natl. Acad. Sci.* **98**, 12357–12361 (2001).
10. Kottke, T., Heberle, J., Hehn, D., Dick, B. & Hegemann, P. Phot-LOV1: photocycle of a blue-light receptor domain from the green alga Chlamydomonas reinhardtii. *Biophys J* **84**, 1192–1201 (2003).
11. Kottke, T., Xie, A., Larsen, D. S. & Hoff, W. D. Photoreceptors Take Charge: Emerging Principles for Light Sensing. *Annu. Rev. Biophys.* https://doi.org/10.1146/annurev-biophys-070317-033047 (2018) doi:10.1146/annurev-biophys-070317-033047.
12. Schleicher, E. *et al.* On the reaction mechanism of adduct formation in LOV domains of the plant blue-light receptor phototropin. *J Am Chem Soc* **126**, 11067–76 (2004).
13. Fedorov, R. *et al.* Crystal structures and molecular mechanism of a light-induced signaling switch: The Phot-LOV1 domain from Chlamydomonas reinhardtii. *Biophys J* **84**, 2474–82 (2003).
14. Olasz, B. *et al.* Covalent bond formation caught in a LOV photoreceptor. 2026.08.02.742302 Preprint at https://doi.org/10.64898/2026.08.02.742302 (2026).
15. Crosson, S. & Moffat, K. Photoexcited structure of a plant photoreceptor domain reveals a light-driven molecular switch. *Plant Cell* **14**, 1067–1075 (2002).

16. Harper, S. M., Neil, L. C. & Gardner, K. H. Structural basis of a phototropin light switch. *Science* **301**, 1541–1544 (2003).
17. Yee, E. F. *et al.* Signal transduction in light-oxygen-voltage receptors lacking the adduct-forming cysteine residue. *Nat. Commun.* **6**, 10079 (2015).
18. Dietler, J. *et al.* Signal transduction in light-oxygen-voltage receptors lacking the active-site glutamine. *Nat. Commun.* **13**, 2618 (2022).
19. García de Fuentes, A. & Möglich, A. Reduction midpoint potential of a paradigm light–oxygen–voltage receptor and its modulation by methionine residues. *RSC Chem. Biol.* **5**, 530–543 (2024).
20. Nöll, G. *et al.* Redox Properties of LOV Domains: Chemical versus Photochemical Reduction, and Influence on the Photocycle. *ChemBioChem* **8**, 2256–2264 (2007).
21. Kennis, J. T. *et al.* Primary reactions of the LOV2 domain of phototropin, a plant blue-light photoreceptor. *Biochemistry* **42**, 3385–92 (2003).
22. Kottke, T. *et al.* Irreversible Photoreduction of Flavin in a Mutated Phot-LOV1 Domain. *Biochemistry* **42**, 9854–9862 (2003).
23. Bittl, R., Kay, C. W. M., Weber, S. & Hegemann, P. Characterization of a flavin radical product in a C57M mutant of a LOV1 domain by electron paramagnetic resonance. *Biochemistry* **42**, 8506–8512 (2003).
24. Losi, A. *et al.* A photochromic bacterial photoreceptor with potential for super-resolution microscopy. *Photochem. Photobiol. Sci. Off. J. Eur. Photochem. Assoc. Eur. Soc. Photobiol.* **12**, 231–235 (2013).
25. Halavaty, A. S. & Moffat, K. N- and C-terminal flanking regions modulate light-induced signal transduction in the LOV2 domain of the blue light sensor phototropin 1 from Avena sativa. *Biochemistry* **46**, 14001–14009 (2007).
26. Guntas, G. *et al.* Engineering an improved light-induced dimer (iLID) for controlling the localization and activity of signaling proteins. *Proc. Natl. Acad. Sci. U. S. A.* **112**, 112–117 (2015).

27. Qi, L. S. *et al.* Repurposing CRISPR as an RNA-guided platform for sequence-specific control of gene expression. *Cell* **152**, 1173–1183 (2013).
28. Möglich, A., Ayers, R. A. & Moffat, K. Design and signaling mechanism of light-regulated histidine kinases. *J. Mol. Biol.* **385**, 1433–1444 (2009).
29. Ohlendorf, R., Vidavski, R. R., Eldar, A., Moffat, K. & Möglich, A. From dusk till dawn: one-plasmid systems for light-regulated gene expression. *J. Mol. Biol.* **416**, 534–542 (2012).
30. Diensthuber, R. P., Bommer, M., Gleichmann, T. & Möglich, A. Full-length structure of a sensor histidine kinase pinpoints coaxial coiled coils as signal transducers and modulators. *Structure* **21**, 1127–1136 (2013).
31. Ohlendorf, R., Schumacher, C. H., Richter, F. & Möglich, A. Library-Aided Probing of Linker Determinants in Hybrid Photoreceptors. *ACS Synth. Biol.* **5**, 1117–1126 (2016).
32. Arinkin, V. *et al.* Dimer asymmetry in signaling of blue light sensor histidine kinases. *Sci. Adv.* **12**, eaed8943 (2026).
33. Weber, A. M. *et al.* A blue light receptor that mediates RNA binding and translational regulation. *Nat Chem Biol* **15**, 1085–1092 (2019).
34. Ranzani, A. T. *et al.* Light-Dependent Control of Bacterial Expression at the mRNA Level. *ACS Synth. Biol.* **11**, 3482–3492 (2022).
35. Pietruschka, G. *et al.* An RNA Motif That Enables Optozyme Control and Light-Dependent Gene Expression in Bacteria and Mammalian Cells. *Adv. Sci. Weinh. Baden-Wurtt. Ger.* e2304519 (2024) doi:10.1002/advs.202304519.
36. Jenal, U., Reinders, A. & Lori, C. Cyclic di-GMP: second messenger extraordinaire. *Nat. Rev. Microbiol.* **15**, 271–284 (2017).
37. Vide, U., Shickle, G., Schwekendiek, J. & Winkler, A. Coiled-coil register transitions and coupling with the effector's inhibitory site enables high fold changes in blue light–regulated diguanylate cyclases. *J. Biol. Chem.* **302**, 111020 (2026).

869 38. Vide, U. *et al.* Illuminating the inner workings of a natural protein switch: Blue-light sensing in
870 LOV-activated diguanylate cyclases. *Sci. Adv.* **9**, eadh4721 (2023).
871 39. Rihakova, L. *et al.* Methionine Proximity Assay, a Novel Method for Exploring Peptide Ligand–
872 Receptor Interaction. *J. Recept. Signal Transduct.* **22**, 297–313 (2002).
873 40. Kim, J. *et al.* Site-Selective Functionalization of Methionine Residues via Photoredox Catalysis.
874 *J. Am. Chem. Soc.* **142**, 21260–21266 (2020).
875 41. Mondal, P., Schwinn, K. & Huix-Rotllant, M. Impact of the redox state of flavin chromophores
876 on the UV–vis spectra, redox and acidity constants and electron affinities. *J. Photochem.*
877 *Photobiol. Chem.* **387**, 112164 (2020).
878 42. Bergès, J., de Oliveira, P., Fourré, I. & Houée-Levin, C. The One-Electron Reduction Potential
879 of Methionine-Containing Peptides Depends on the Sequence. *J. Phys. Chem. B* **116**, 9352–9362
880 (2012).
881 43. Yao, X., Rosen, M. K. & Gardner, K. H. Estimation of the available free energy in a LOV2-J
882 alpha photoswitch. *Nat. Chem. Biol.* **4**, 491–497 (2008).
883 44. Möglich, A. Signal transduction in photoreceptor histidine kinases. *Protein Sci.* **28**, 1923–1946
884 (2019).
885 45. Pudasaini, A., El-Arab, K. K. & Zoltowski, B. D. LOV-based optogenetic devices: light-driven
886 modules to impart photoregulated control of cellular signaling. *Front. Mol. Biosci.* **2**, 18 (2015).
887 46. Patterson, G. H. & Lippincott-Schwartz, J. A Photoactivatable GFP for Selective Photolabeling
888 of Proteins and Cells. *Science* **297**, 1873–1877 (2002).
889 47. Ortiz-Guerrero, J. M., Polanco, M. C., Murillo, F. J., Padmanabhan, S. & Elías-Arnanz, M. Light-
890 dependent gene regulation by a coenzyme B12-based photoreceptor. *Proc. Natl. Acad. Sci. U. S.*
891 *A.* **108**, 7565–7570 (2011).
892 48. Gibson, D. G. *et al.* Enzymatic assembly of DNA molecules up to several hundred kilobases. *Nat.*
893 *Methods* **6**, 343–345 (2009).

894 49. Mathes, T., Vogl, C., Stolz, J. & Hegemann, P. In vivo generation of flavoproteins with modified
895 cofactors. *J. Mol. Biol.* **385**, 1511–1518 (2009).
896 50. Andersen, K. R., Leksa, N. C. & Schwartz, T. U. Optimized E. coli expression strain LOBSTR
897 eliminates common contaminants from His-tag purification. *Proteins Struct. Funct. Bioinforma.*
898 **81**, 1857–1861 (2013).
899 51. Yi, C., Meier, S. S. M., Kehr, M. & Möglich, A. Spectroscopic Analyses of Photoconversion in
900 Phytochromes. *Methods Mol. Biol.* **2970**, 177–191 (2026).
901 52. Möglich, A. An Open-Source, Cross-Platform Resource for Nonlinear Least-Squares Curve
902 Fitting. *J. Chem. Educ.* **95**, 2273–2278 (2018).
903 53. Kabsch, W. XDS. *Acta Crystallogr. D Biol. Crystallogr.* **66**, 125–132 (2010).
904 54. Krug, M., Weiss, M. S., Heinemann, U. & Mueller, U. XDSAPP: a graphical user interface for
905 the convenient processing of diffraction data using XDS. *J. Appl. Crystallogr.* **45**, 568–572
906 (2012).
907 55. McCoy, A. J. *et al.* Phaser crystallographic software. *J. Appl. Crystallogr.* **40**, 658–674 (2007).
908 56. Emsley, P. & Cowtan, K. Coot: model-building tools for molecular graphics. *Acta Crystallogr. D*
909 *Biol. Crystallogr.* **60**, 2126–2132 (2004).
910 57. Murshudov, G. N. *et al.* REFMAC5 for the refinement of macromolecular crystal structures. *Acta*
911 *Crystallogr. D Biol. Crystallogr.* **67**, 355–367 (2011).
912 58. Chen, V. B. *et al.* MolProbity: all-atom structure validation for macromolecular crystallography.
913 *Acta Crystallogr. D Biol. Crystallogr.* **66**, 12–21 (2010).
914 59. Hennemann, J. *et al.* Optogenetic Control by Pulsed Illumination. *Chembiochem* **19**, 1296–1304
915 (2018).
916 60. Crosson, S., Rajagopal, S. & Moffat, K. The LOV domain family: photoresponsive signaling
917 modules coupled to diverse output domains. *Biochemistry* **42**, 2–10 (2003).
918 61. Eddy, S. R. Profile hidden Markov models. *Bioinformatics* **14**, 755–763 (1998).
919 62. Finn, R. D. *et al.* Pfam: clans, web tools and services. *Nucleic Acids Res* **34**, D247–D251 (2006).

63. Larkin, M. A. *et al.* Clustal W and Clustal X version 2.0. *Bioinformatics* **23**, 2947–2948 (2007).
64. Edgar, R. C. MUSCLE: multiple sequence alignment with high accuracy and high throughput. *Nucleic Acids Res.* **32**, 1792 (2004).
65. Crooks, G. E., Hon, G., Chandonia, J.-M. & Brenner, S. E. WebLogo: A Sequence Logo Generator. *Genome Res.* **14**, 1188–1190 (2004).

Acknowledgements

We thank our coworkers and Dr. A. Musacchio for discussion; J. Koch for initial experiments on LOVme-Dusk; and Dr. M. Weyand for advice on X-ray crystallography. Funding was provided by the German Research Foundation (grants MO2192/8-2 and MO2192/10-1 to A.M.; grant MA3442/9-1 to G.M.). This work is further supported by ERC grant IntraMAP (101140898) to G.M., funded by the European Union. Views and opinions expressed are however those of the author(s) only and do not necessarily reflect those of the European Union or the European Research Council Executive Agency. Neither the European Union nor the granting authority can be held responsible for them.

Author Contributions

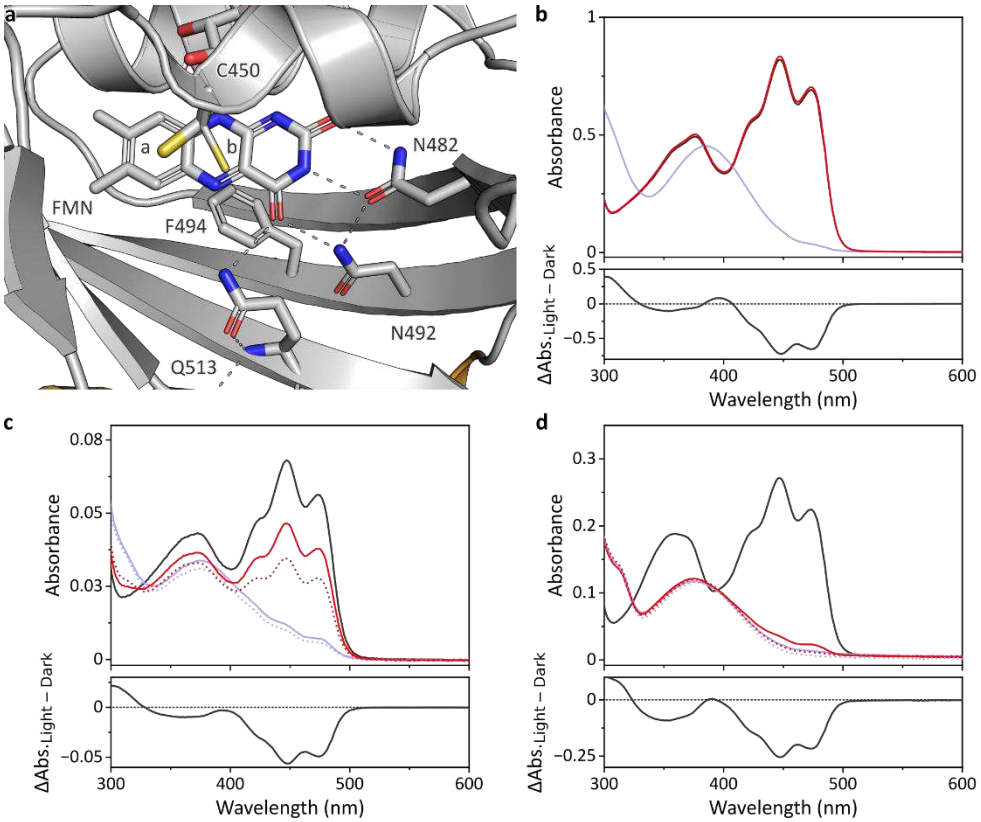
L.O. and A.M. conceived of the project. G.M. & A.M. acquired funding. L.O., A.T.R., M.B., A.K., C.R., O.B., A.G.F., T.K., & A.M. performed and evaluated experiments. C.W. & I.S. contributed to discussion of results. C.U., G.M., & A.M. supervised the project. L.O., A.K., & A.M. prepared figures. L.O. and A.M. wrote the manuscript with input from all authors.

Competing Interests

The authors declare no competing interests.

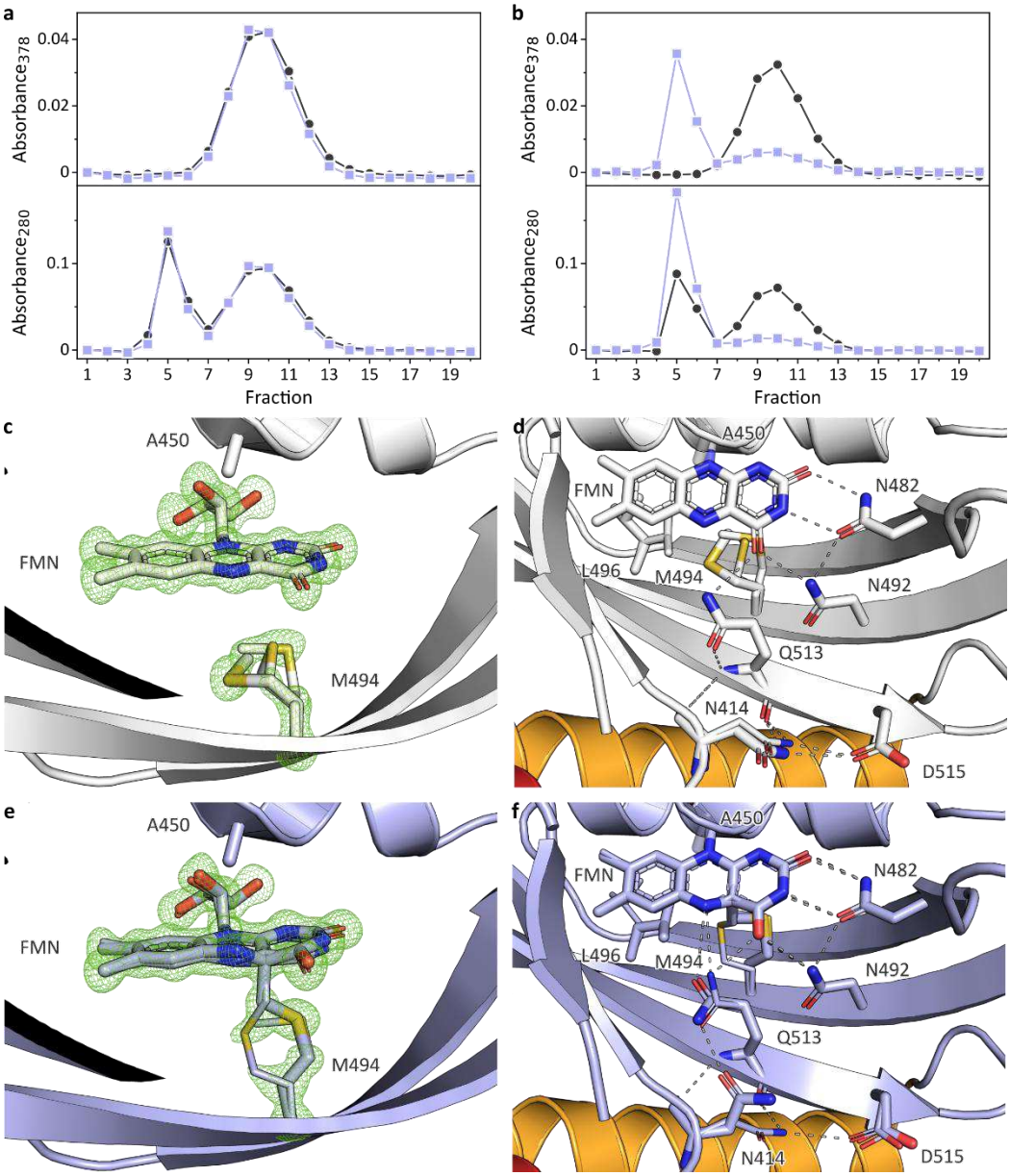
Figures

Figure 1



A methionyl-flavin photoadduct in a paradigm light-oxygen-voltage (LOV) receptor. **a**, Chromophore-binding pocket of the LOV2 domain of *Avena sativa* phototropin 1 LOV2 (*As*LOV2, [18]). The flavin chromophore and select residues, including phenylalanine 494 and the conserved cysteine 450 and glutamine 513, are highlighted as sticks. **b**, UV-vis absorbance spectra of *As*LOV2 recorded for the dark-adapted sample (black line), after blue-light exposure (blue), and upon ensuing recovery in darkness (red). The lower panel shows a light-minus-dark difference spectrum. **c**, As in panel b but for *As*LOV2 with phenylalanine 494 replaced by methionine. The solid and dotted lines denote spectra obtained after 2 and 4 cycles, respectively, of blue-light exposure (blue) followed by thermal recovery (red). **d**, As in panel c but for the *As*LOV2 variant C450A:F494M with cysteine 450 additionally substituted by alanine. The solid and dotted lines refer to data acquired for the first and second illumination-recovery cycles

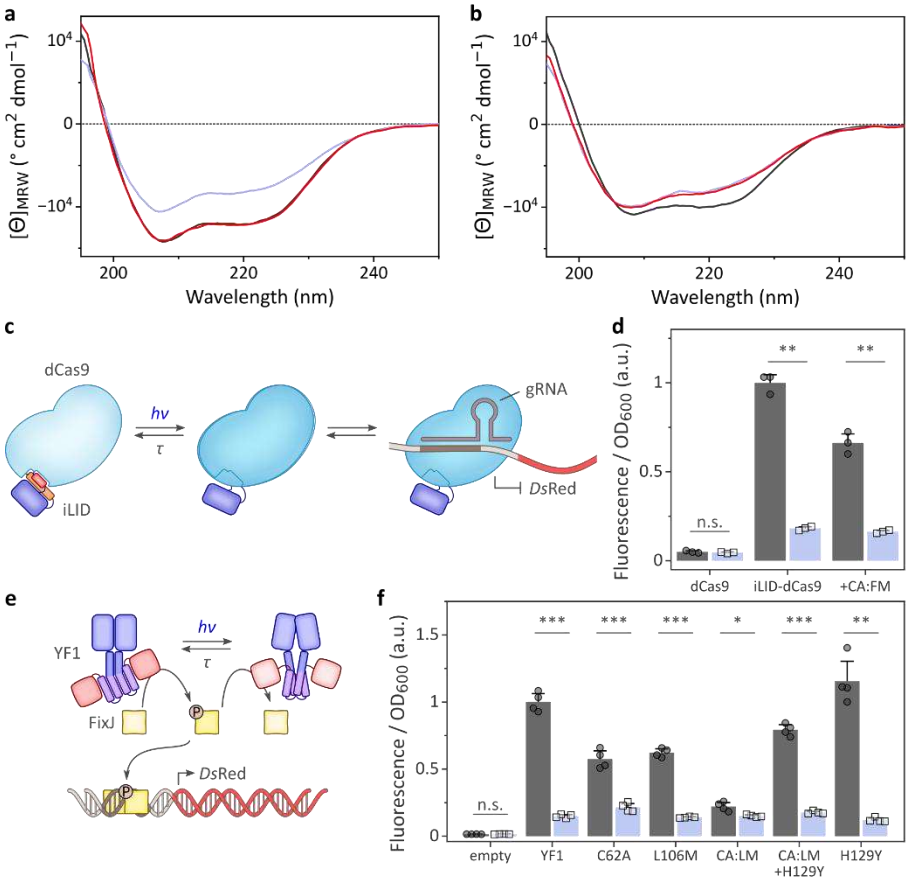
Figure 2



Nature of the methionyl-flavin Cε-C4a photoadduct in LOVme receptors. **a**, Analyses by size-exclusion chromatography (SEC) of *Avena sativa* phototropin 1 LOV2 (*As*LOV2) after incubation in darkness (grey symbols) vs. blue light (blue symbols). Prior to chromatography, the samples were denatured by guanidinium chloride. The elution of the flavin chromophore was tracked at 378 nm (upper panel), and that of the protein moiety plus flavin at 280 nm (lower panel). **b**, As panel a but for *As*LOV2 CA:FM. **c**, Close-up view of the flavin-binding pocket of dark-adapted *As*LOV2 CA:FM with the chromophore and select residues shown as sticks. For residues exhibiting multiple conformations, the major and minor ones are indicated by wide and narrow sticks, respectively. The green mesh denotes a *Fo-Fc* omit electron density map contoured at +3.0 σ. **d**, Residues involved in

signal transduction within dark-adapted *As*LOV2 CA:FM. For better visibility, the helices Cα and Dα are omitted from the display. **e**, As panel c but for the pseudo-light structure of *As*LOV2 CA:FM. **f**, As panel d but for the pseudo-light structure of *As*LOV2 CA:FM.

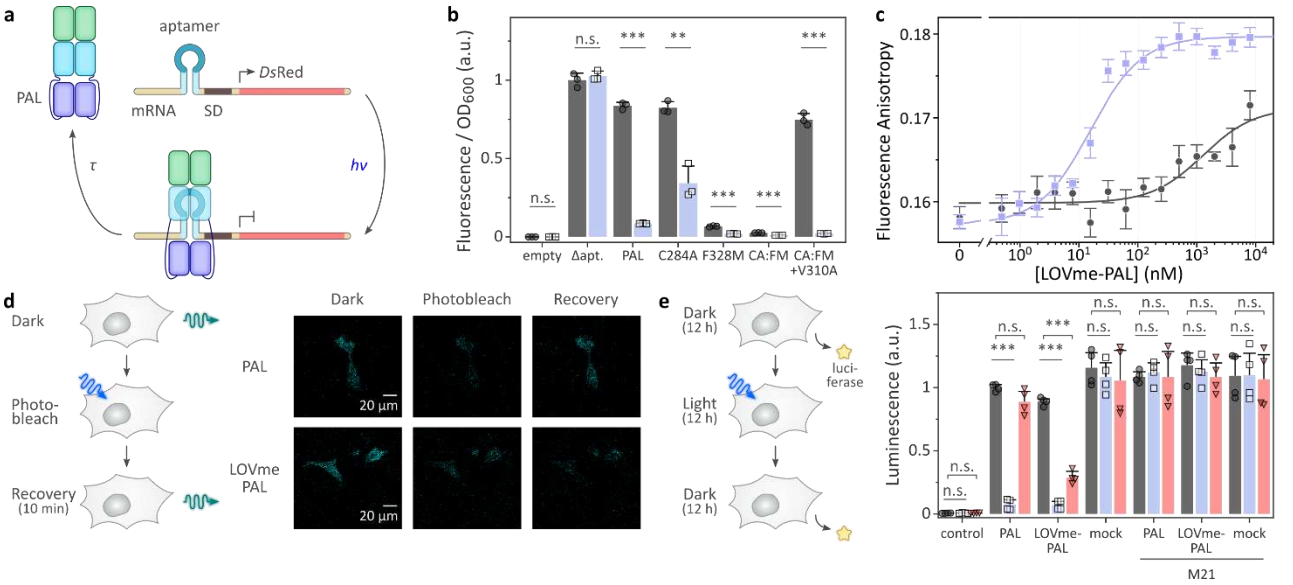
Figure 3



Signal transduction in LOVme blue-light receptors. **a**, Far-UV circular dichroism spectra of wild-type *Avena sativa* phototropin 1 LOV2 (*As*LOV2) in the dark-adapted state (black line), immediately upon exposure to blue light (blue), and after recovery in darkness (red). **b**, As in panel a but for *As*LOV2 C450A:F494M. **c**, Schematic of iLID-dCas9 and its blue-light-dependent regulation of bacterial expression. The insertion of the derivative *As*LOV2 domain iLID into a surface-exposed helix renders dCas9 little active in darkness. Blue light promotes the partial α-helical unfolding of iLID and thereby releases iLID-dCas9 autoinhibition, enables sequence-specific DNA binding, and incurs repression of the red-fluorescent *Ds*Red reporter gene. **d**, *Escherichia coli* bacteria harboring the iLID-dCas9 reporter setup were incubated in darkness or under blue light, followed by measurements of optical density at 600 nm (OD_{600}) and *Ds*Red fluorescence. Fluorescence readings were divided by OD_{600} and normalized to the values obtained for the original iLID-dCas9 in darkness. Data represent mean ± s.d. of 3 biological replicates, shown as individual symbols. **e**, Schematic of the pDusk reporter-gene setup. In its dark-adapted state, the engineered LOV receptor YF1 acts as a net histidine kinase

on its cognate response regulator FixJ which in turn binds to a specific promoter and thereby activates the expression of the red-fluorescent *Ds*Red. Under blue light, YF1 becomes a net phosphatase, and *Ds*Red reporter fluorescence is repressed. **f**, *E. coli* bacteria harboring the pDusk-*Ds*Red setup were incubated in darkness or blue light, followed by measurements of reporter fluorescence and OD_{600} of the bacterial culture. Fluorescence data were normalized to OD_{600} and the reference value observed for the original YF1 when incubated in darkness. Data represent mean ± s.d. of 4 biological replicates, individually shown as circles and squares. Symbols above the bars in panels d and f denote results from Welch's two-sided *t*-tests for the pairwise comparison of dark vs. light conditions (n.s. not significant, * $p < 0.05$, ** $p < 0.01$, *** $p < 0.001$).

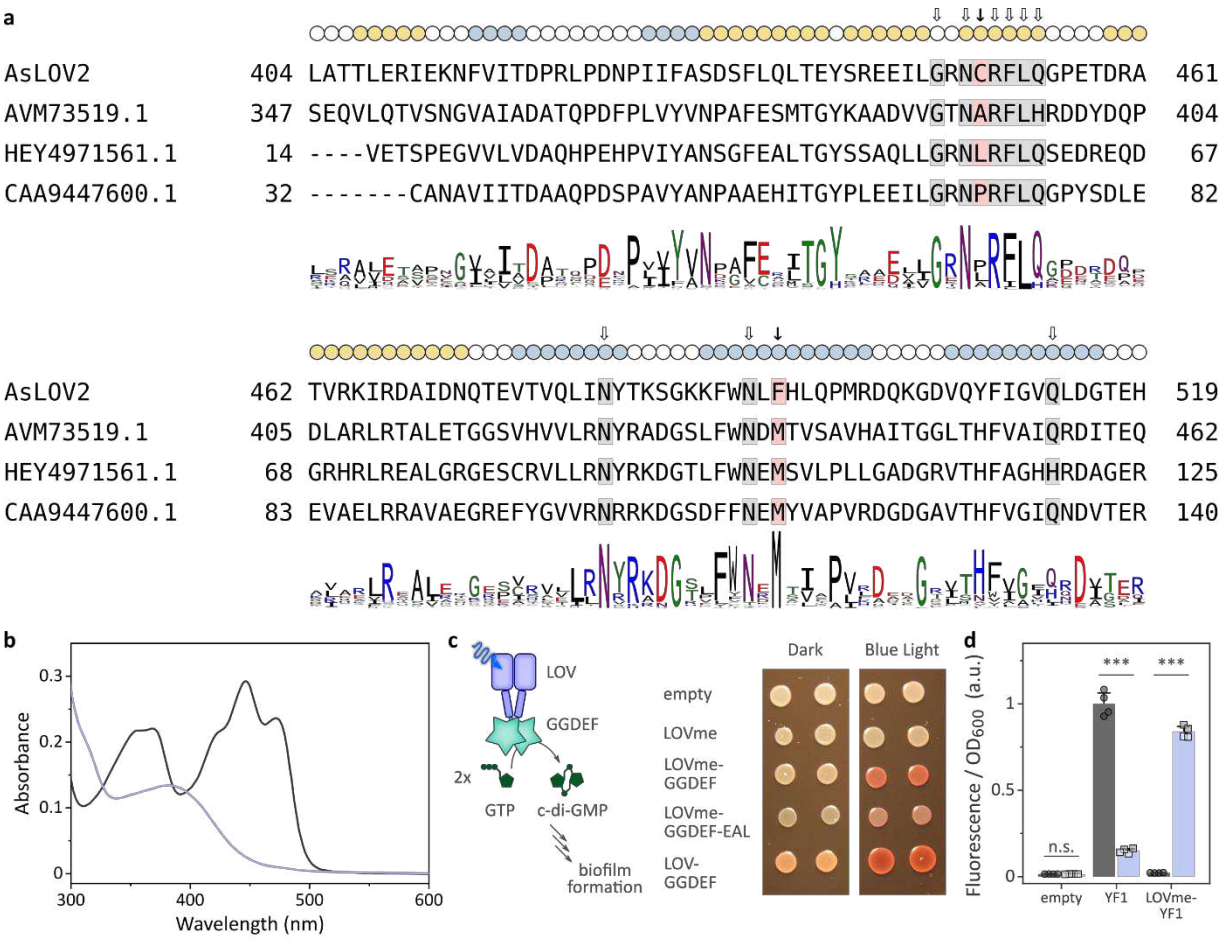
Figure 4



Light-induced RNA binding and optoribogenetics by a LOVme receptor. **a**, Schematic of the pCrepusculo reporter-gene setup. Activated by blue light, the LOV receptor PAL sequence-specifically binds a short RNA hairpin, termed aptamer, embedded near the ribosome-binding site (SD) of a bacterial mRNA encoding the red-fluorescent reporter *Ds*Red. Expression is thereby hindered, and a lower fluorescence than in darkness results. **b**, *E. coli* bacteria carrying pCrepusculo-*Ds*Red were incubated in darkness (grey bars) or under blue light (light blue). The resultant *Ds*Red fluorescence was divided by the optical density of the culture at 600 nm and normalized to the reading of wild-type PAL in darkness. Data reflect mean ± s.d. of 3 biological replicates, individually shown as circles and squares. MCS and Δaptamer denote empty-vector control and a pCrepusculo derivative altogether lacking the aptamer, respectively. **c**, A fluorescently labeled RNA aptamer was incubated with increasing concentrations of dark-adapted LOVme-PAL, followed by measurements of fluorescence anisotropy (grey symbols). Upon exposure to blue light, the anisotropy was recorded again (blue). Solid lines denote fits to single-site binding isotherms. **d**, Upon stable expression in HeLa cells, the fluorescence of wild-type PAL and its LOVme variant was assessed by fluorescence microscopy [33]. Photobleaching by strong blue light incurs photoactivation of PAL and a reduction of the observable green flavin fluorescence. For wild-type PAL but not for LOVme-PAL, the initial fluorescence signal recovers upon 10 min incubation in darkness. **e**, Wild-type PAL and the LOVme

variant were embedded into an optoribogenetic circuit for the expression control of a secreted luciferase (see Suppl. Fig. 17d). HeLa cells harboring the circuit were incubated for 12 h each in darkness (grey bars), under blue light (blue), and finally again in darkness (red). At each step, the reporter luminescence was determined and normalized to the value obtained for wild-type PAL in darkness. Data represent mean ± s.d. of 4 biological replicates shown as circles, squares, and triangles. Mock refers to HeLa cells not expressing any PAL variant; M21 denotes a mutation within the aptamer that greatly lowers the affinity for the PAL receptor. Symbols above the bars in panels b and e denote results from two-sided *t*-tests for comparisons between the individual conditions (n.s. not significant, * $p < 0.05$, ** $p < 0.01$, *** $p < 0.001$).

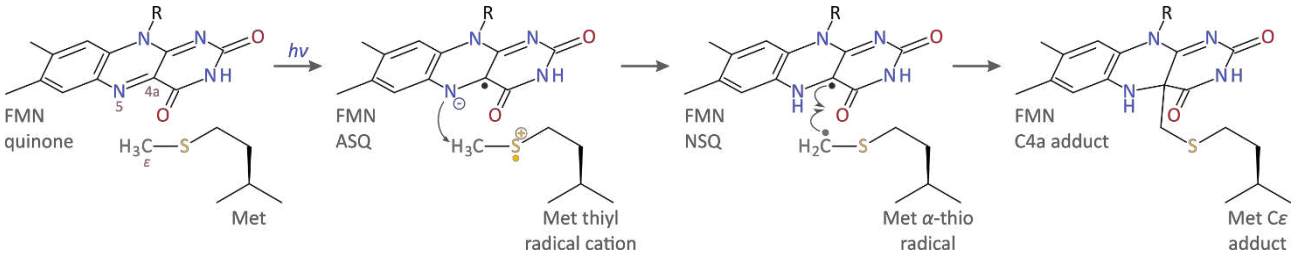
Figure 5



LOVme receptors in nature. **a**, Sequence analyses identify some 50 candidate receptors in GenBank exhibiting the key sequence motifs associated with LOVme signal transduction. Grey shading and open arrows highlight residues strongly conserved across canonical LOV receptors [60]; red shading and black arrows mark the adduct-forming cysteine and methionine residues of canonical LOV and LOVme receptors, respectively. The multiple sequence alignment shows three select LOVme candidates compared to the paradigm *Avena sativa* phototropin 1 LOV2 (*As*LOV2), the secondary structure of which is indicated on top (tan, blue, and white circles denote α-helical, β-sheet, and loop elements). The sequence logo below is based on a complete alignment of all the LOVme receptors identified (Suppl. Fig. 19a). **b**, UV/vis absorbance spectra of the naturally occurring LOVme domain from the *Rubrobacteraceae* LOVme-GGDEF-EAL protein in its dark-adapted state (black line) and after blue-light exposure (blue). **c**, *Escherichia coli* bacteria expressing the *Rubrobacteraceae* LOVme-GGDEF-EAL receptor or the truncated LOVme and LOVme-GGDEF constructs were

cultivated in darkness or under blue light. Biofilm formation triggered by intracellular cyclic-di-GMP production was assessed in the respective bacterial colonies on agar plates by Congo Red staining. As an additional control, the canonical LOV-GGDEF receptor *Ms*LadC [38] was analyzed in parallel. Reflectance measurements of the bacterial colonies are provided in Suppl. Fig. 20b-e. **d**, The *Rubrobacteraceae* LOVme domain was introduced into the pDusk reporter setup, and the response to blue light of the resultant LOVme-Dusk system was probed by reporter fluorescence measurements (see Fig. 3e-f). Symbols above the bars denote results from Welch's two-sided *t*-tests for the pairwise comparison of dark vs. light conditions (n.s. not significant, * $p < 0.05$, ** $p < 0.01$, *** $p < 0.001$).

Figure 6



Proposed mechanism of methionyl-flavin Cε-C4a photoadduct formation in LOVme receptors. Electronic excitation renders the flavin chromophore a strong oxidant that can abstract an electron from the nearby sulfur atom of methionine to produce the flavin anionic semiquinone (ASQ) and a thiyl radical cation. Said radical cation stabilizes to a neutral α-thio radical by deprotonation at its Cε methyl group. Formally, the ASQ can serve as the proton acceptor in this reaction and thereby converts to the neutral semiquinone (NSQ). As a final step, the radical pair recombines to form a carbon-carbon bond between the methionine Cε and the flavin C4a atoms.

Supplementary Files

This is a list of supplementary files associated with this preprint. Click to download.

- LOVmedoosifinnocode.pdf